This is the author-created version of the research project:

Cohesive Micromechanics for Damage Modeling of Composite Materials and Structures

A. Matzenmiller, M. Schmerbauch, M. Donhauser

Institute of Mechanics
Department of Mechanical Engineering
University of Kassel
Mönchebergstr. 7
34125 Kassel
Germany

Phone: +49 561 804 2044
Fax: +49 561 804 2720
amat@uni-kassel.de

in cooperation with

J. Aboudi, R. Haj-Ali, A. Levi-Sasson

School of Mechanical Engineering
Faculty of Engineering
University of Tel-Aviv
Ramat-Aviv, 6997801
Israel

Project period: 01.01.2013 - 31.12.2015

Table of Contents

1 Introduction

M. Donhauser, M. Schmerbauch, A. Matzenmiller

The failure prediction of composites is still a current research task since various macro- and micromechanical approaches can not predict well all complex damage mechanisms. Kaddour, Hinton, Smith and Li [16] state the apt question: *"How well can we predict damage in composites?"*. The complicated (complex) failure mechanisms at the macro scale are postponed to the elementary failure mechanisms at the micro scale:

- matrix-fiber debonding
- matrix cracking
- fiber rupture

A multiphase composite is shwon at both scales in Fig. 1.0-1. The Generalized Method of Cells (GMC) and the High-Fidelity Generalized Method of Cells (HFGMC) as micromechanical approaches, see for an overview [2], have been developed for the analysis of multiphase composite materials. Both methods are based on the homogenization technique for periodic composites and are able to determine local field quantities as well as the effective material behavior. The failure mechanisms can be modeled by using the

- element deletion method
- inter-element crack method
- remeshing technique for crack growth
- Extended Finite-Element-Method (XFEM), see [7].

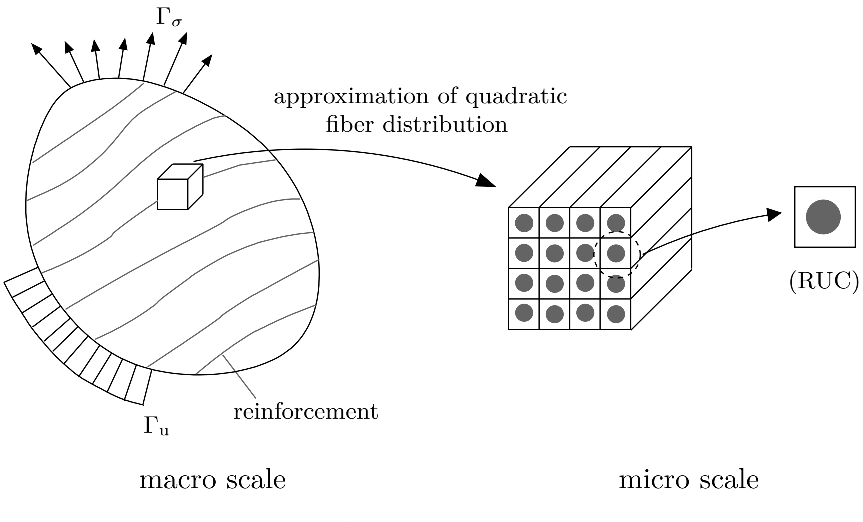

Fig. 1.0-1: Unidirectional periodic array of multiphase composite media with its repeating unit cell (RUC)

Moreover, the inter-element crack method can capture crack initiation as the traction separation models comprise a damage model to represent damage in several sections of a material body.

The XFEM is based on the formulation of the FEM and has an extended displacement approach which allows representing cracks mesh independent. This research report comprises the micromechanical modeling of damage and failure using the concept of cohesive interface damage applied to the HFGMC and the multiscale coupling with the XFEM at the macro scale.

The report is structured based on the research tasks of the project as follows:
Chapter 2 shows the comparison of homogenization results for different load cases using the GMC, HFGMC and FEM, after a brief introduction of all approaches. This research task has been processed in a preliminary stage of the research project and was published in [22]. (Research task: UKSL-1.1)

The regular HFGMC with cohesive interface damage is presented in Chapter 3 in its condensed form with all necessary equations. A structured assembling of the resultant nonlinear system of equations is conducted by using the direct stiffness method well-known from the assembling procedure of the FEM. Afterwards, two solution methods, the consistent linearization and weak coupling, are shown and checked against each other. A study reveal the loss of convergence for certain model parameters if the consistent linearization technique is used, which can be avoided by using weak-coupling-relation among the constitutive equations of the traction-separation-law.(Research task: UKSL-1.2 and UKSL-1.3)

Chapter 4 contains the description of the Extended Finite-Element-Method (XFEM) and the multiscale analysis. The discretization approach by the XFEM and the resulting finite element types are introduced. The element stiffness matrix for the cut element and the crack tip element are deduced. In a first step, a multiscale analysis of a cracked plate under Mode-I loading using the linear elastic HFGMC at the micro scale is shown and compared to the analytical solution, which moreover verifies the implementation of the XFEM and the interaction between both scales. (Research task: UKSL-1.4 and UKSL-2.1)

2 Comparison of Cell Approach with Finite-Element-Method

M. Schmerbauch, M. Donhauser, A. Matzenmiller

2.1 Homogenization Methods

2.1.1 Finite Element Method

The weak form of the static equilibrium equation is given by

$$\int\limits_{\Omega} \delta\boldsymbol{\epsilon} : \boldsymbol{\sigma} \mathrm{d}V = \int\limits_{\Omega} \delta\mathbf{u} \cdot \rho\mathbf{f} \mathrm{d}V + \int\limits_{\Gamma} \delta\mathbf{u} \cdot \mathbf{t} \mathrm{d}A \tag{2.1-1}$$

where the integral on the left hand side is the internal virtual work and the integrals on the right hand side are the external virtual works due to body forces and prescribed tractions. The discretization of Eq. (2.1-1) by the Finite-Element-Method leads to

$$\bigcup_{\mathrm{e}=1}^{n_\mathrm{e}} \delta\mathbf{u}^\mathsf{T} \int\limits_{\Omega_\mathrm{e}} \mathbf{B}^\mathsf{T}\mathbf{C}\mathbf{B}\mathbf{u} \mathrm{d}V = \bigcup_{\mathrm{e}=1}^{n_\mathrm{e}} \delta\mathbf{u}^\mathsf{T} \Big(\int\limits_{\Omega_\mathrm{e}} \mathbf{N}^\mathsf{T}\rho\mathbf{f} \mathrm{d}V + \int\limits_{\Gamma_\mathrm{e}} \mathbf{N}^\mathsf{T}\mathbf{t} \mathrm{d}A \Big) \tag{2.1-2}$$

where small deformations and linear elastic material behavior are assumed, for details see [7]. In order to determine the stress and strain fields in the RUC by the finite element analysis a approximation of the averaged stress energy is required

$$\langle U^h \rangle = \frac{1}{2V_\mathrm{RVE}} \int\limits_{\partial\Omega_\mathsf{RVE}} \boldsymbol{\sigma}^h : \boldsymbol{\epsilon}^h \, \mathrm{d}\Omega \ . \tag{2.1-3}$$

The specific strain energy of the homogenized continuum is given by

$$U^* = \frac{1}{2}\langle \boldsymbol{\sigma} \rangle : \langle \boldsymbol{\epsilon} \rangle = \frac{1}{2}\langle \boldsymbol{\epsilon} \rangle : \mathbf{C}^* : \langle \boldsymbol{\epsilon} \rangle, \tag{2.1-4}$$

where $\mathbf{C}^*$ is the unknown effective stiffness tensor. Using Hill's theorem of macro homogeneity both strain energies can be equated

$$U^* = \langle U^h \rangle \tag{2.1-5}$$

$$\frac{1}{2}\langle \boldsymbol{\epsilon} \rangle : \mathbf{C}^* : \langle \boldsymbol{\epsilon} \rangle = \frac{1}{2V_\mathrm{RVE}} \int\limits_{\partial\Omega_\mathrm{RVE}} \boldsymbol{\sigma}^h : \boldsymbol{\epsilon}^h \, \mathrm{d}\Omega = \langle U^h \rangle \ . \tag{2.1-6}$$

Hence, the effective stiffness tensor $\mathbf{C}^*$ can be determined from the solutions of $\boldsymbol{\sigma}^h$ and $\boldsymbol{\epsilon}^h$ for six applied load cases (LC), where one strain component is set to unity while the other are kept zero [22]. For instance, the effective stiffness C^*_{22} and C^*_{44} are determined by

$$\frac{1}{2} C^*_{22} {\epsilon^0_{22}}^2 \ |_\mathrm{LC\,II} = \langle U^h \rangle \ |_\mathrm{LC\,II} \tag{2.1-7}$$

$$\frac{1}{2} C^*_{44} {\epsilon^0_{23}}^2 \ |_\mathrm{LC\,IV} = \langle U^h \rangle \ |_\mathrm{LC\,IV} \ . \tag{2.1-8}$$

2.1.2 Generalized Method of Cells

The GMC, see [24] and [1], is a semianalytical homogenization method for periodic microstructures assuming a first order displacement approach

$$\mathbf{u}^{(\alpha\beta\gamma)} = \mathbf{w}^{(\alpha\beta\gamma)} + \mathbf{\Phi}^{(\alpha\beta\gamma)} z_1^{(\alpha\beta\gamma)} + \mathbf{\Psi}^{(\alpha\beta\gamma)} z_2^{(\alpha\beta\gamma)} + \mathbf{\Xi}^{(\alpha\beta\gamma)} z_3^{(\alpha\beta\gamma)} \tag{2.1-9}$$

where $\mathbf{w}^{(\alpha\beta\gamma)}$, $\mathbf{\Phi}^{(\alpha\beta\gamma)}$, $\mathbf{\Psi}^{(\alpha\beta\gamma)}$ and $\mathbf{\Xi}^{(\alpha\beta\gamma)}$ are the microvariables and imposing traction and displacement continuity in an average sense. Based on a spatial discretization of a RUC into an arbitrary number of rectangular subcells $\Omega^{(\alpha\beta\gamma)}$, the traction and displacement conditions imposed lead to a linear system of equations for the surface-averaged normal stresses T_{ii}

$$\mathbf{ST} = \mathbf{K}\langle\epsilon\rangle \tag{2.1-10}$$

and to explicit equations for the shear-stress T_{ij} with $i \neq j$, see [2]. In Eq. (2.1-10) $\mathbf{T}$ is the hyper-vector of the normal stresses, $\mathbf{S}$ is defined by the geometry and stiffness values of all subcells, $\langle\epsilon\rangle$ by the boundary conditions and $\mathbf{K}$ by the dimensions of the RUC, see [25] and [22]. The effective stiffness $\mathbf{C}^*$ is given by the partial derivative of the macro stress $\langle\sigma_i\rangle$ with respect to the macro strain $\langle\epsilon_j^0\rangle$

$$C_{ij}^* = \frac{\partial\langle\sigma_i\rangle}{\partial\langle\epsilon_j^0\rangle} \ . \tag{2.1-11}$$

After conducting the derivative Eq. (2.1-11) yields an explicit expression for the components of the effective stiffness tensor, for instance C_{22}^* and C_{44}^*, see Aboudi [2].

$$C_{22}^* = \sum_{\alpha=1}^{N_\alpha}\sum_{\gamma=1}^{N_\gamma} \frac{d_\alpha d_\gamma}{dl} C_{22}^{\hat{\alpha\gamma}} \tag{2.1-12}$$

$$C_{44}^* = \frac{hl}{d}\sum_{\alpha=1}^{N_\alpha}\sum_{\beta=1}^{N_\beta}\sum_{\gamma=1}^{N_\gamma} \frac{d_\alpha}{h_\beta l_\gamma S_{44}^{(\alpha\beta\gamma)}} \tag{2.1-13}$$

2.1.3 High Fidelity Generalized Method of Cells

The GMC has the lack of shear coupling since this effect can become a first-order effect not captured by the linear approach of the displacement field within a subcell $\Omega^{(\beta\gamma)}$. Hence, the HFGMC uses a second-order approach

$$\begin{aligned}\mathbf{u}^{(\beta,\gamma)} &= \bar{\mathbf{u}} + \mathbf{W}_{(00)}^{(\beta,\gamma)} + z_2^{(\beta,\gamma)}\mathbf{W}_{(10)}^{(\beta,\gamma)} + z_3^{(\beta,\gamma)}\mathbf{W}_{(01)}^{(\beta,\gamma)} + \\ &+ \frac{1}{2}\left[3\left(z_2^{(\beta,\gamma)}\right)^2 - \frac{\left(l_2^{(\beta)}\right)^2}{4}\right]\mathbf{W}_{(20)}^{(\beta,\gamma)} + \frac{1}{2}\left[3\left(z_3^{(\beta,\gamma)}\right)^2 - \frac{\left(l_3^{(\gamma)}\right)^2}{4}\right]\mathbf{W}_{(02)}^{(\beta,\gamma)} \ ,\end{aligned} \tag{2.1-14}$$

where $\mathbf{W}^{(\beta,\gamma)}$ are the unknown microvariables. Applying the traction and displacement continuity in its average sense to a discretized RUC with an arbitrary number of rectangular subcells leads to a resultant linear system of equations for linear-elastic material behavior of the micro constituents. The method in its original formulation solves the system of equations for the microvariables $\mathbf{W}$, see [3], whereby a condensed form with a fewer number of unknowns, the surface-averaged displacements $\bar{\mathbf{u}}'^{(\beta\gamma)}$, exists, see [14], [5], [2], which is used:

$$\hat{\mathbf{K}}\bar{\mathbf{u}}' = -\mathbf{D}\boldsymbol{\epsilon}^0 \ . \tag{2.1-15}$$

The effective stiffness $\mathbf{C}^*$, see Eq. (2.1-16), results from a weighted summation of subcell stiffness $\mathbf{C}^{(\beta\gamma)}$ multiplied with its corresponding strain concentration tensor $\mathbf{A}^{(\beta\gamma)}$:

$$\mathbf{C}^* = \frac{1}{HL} \sum_{\gamma=1}^{N_\gamma} \sum_{\beta=1}^{N_\beta} h_\beta h_\gamma \mathbf{C}^{(\beta\gamma)} \mathbf{A}^{(\beta\gamma)} \qquad (2.1\text{-}16)$$

2.2 Comparison of Results

Different two-dimensional discretizations, see Fig. 2.2-1, of the RUC with a single fiber (volume content $v_f = 0.5$) surrounded by matrix material are considered under transverse normal and shear loading to predict the homogenized stiffness C^*_{22} and C^*_{44}. The results are obtained for

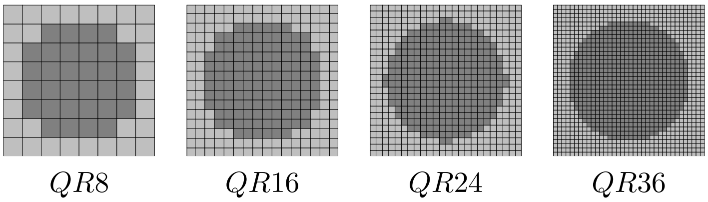

Fig. 2.2-1: Different discretizations of RUC with quadratic subcells (QR) [22]

homogeneous and periodic boundary conditions. The elastic material parameters of the transverse isotropic carbon fiber are $E_a = 220.7$ GPa, $E_t = 72.4$ GPa, $G_a = 6.9$ GPa, $G_t = 10.3$ GPa, $\nu_t = 0.25$ and of the isotropic epoxy resin $E = 3.2$ GPa and $G = 1.2$ GPa, see [4]. The commercial program ANSYS is used for the homogenization with the FEM where the finite element PLANE42 is chosen for a state of plane strain. To improve the accuracy of the coarse mesh, the option extra displacement shapes (EDS) is enabled in the element formulation. The homogenization results are shown in Fig. 2.2-2, which depend on the number of used elements. The finite element analysis with homogeneous boundary conditions provides the highest effective

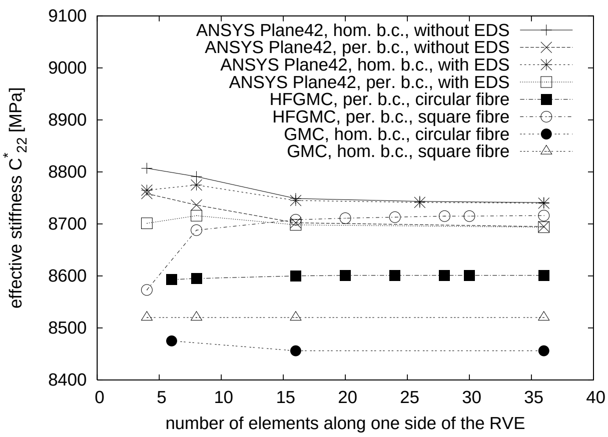

Fig. 2.2-2: Effective transverse stiffness C^*_{22} obtained by different micromechanical approaches [22]

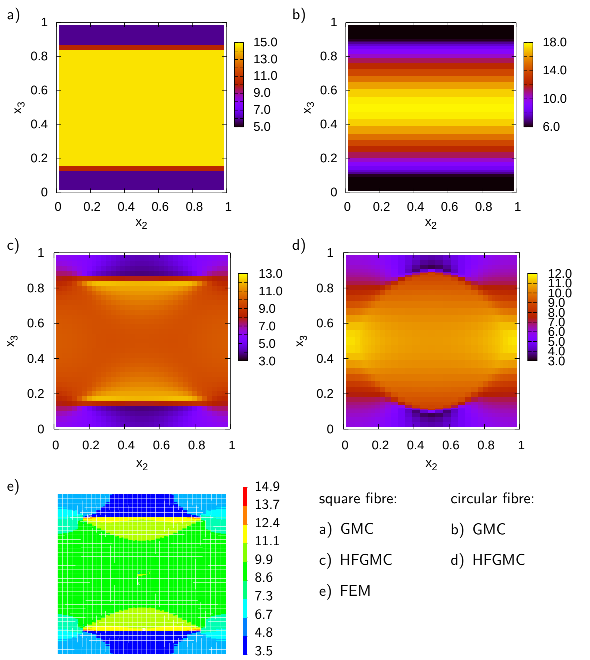

Fig. 2.2-3: Predicted stress distribution σ_{22} in GPa for $\epsilon_{22} = 1$ [22]

stiffness C^*_{22} whether or not the option EDS is active, see Fig. 2.2-2 a. Applying periodic boundary conditions instead of homogeneous one, the effective stiffness decrease only slightly. A finer mesh in the HFGMC analysis predicts a stiffness which is between the results of the finite element analysis under homogeneous and periodic boundary conditions. The GMC analysis yields the lowest results because of the approximately homogeneous stress distribution (Fig. 2.2-3 a-b) as a result of the linear displacement approach (2.1-9), for details see [2]. The distribution of normal stress σ_{22} of the FEM and HFGMC corresponds quite well, see Fig. 2.2-3e and 2.2-3c. The discretization of the fiber cross section has a heavy influence on the stress distribution, as shown in Fig. 2.2-3c and Fig. 2.2-3d. The maximal stress σ_{22} is located at the corners for the square fiber geometry and at the horizontal line for the circular geometry. The depiction of the circular fibre geometry leads to a reducing stiffness for both cell methods.
The homogenization results of the transverse shear stiffness C^*_{44} are illustrated in Fig. 2.2-4. The finite element analysis predicts the highest effective transverse shear stiffness with and without using the EDS option. The boundary conditions have a significant influence again such as in the previous case. The effective shear stiffness obtained by the HFGMC under homogeneous boundary conditions lies between the FEM results with homogeneous and periodic boundary conditions. The fibre shape discretization has for the cell methods only a small influence on the effective shear stiffness C^*_{44}. The homogeneous stress distribution of the GMC models (Fig. 2.2-5a-b) leads to the lowest shear stiffness, which are independent of the number of used elements and the fiber geometry. As shown in Fig. 2.2-5c-d the fiber shape affects the stress distribution for the HFGMC. However, the stress distribution of the HFGMC and the FEM for a square fiber are nearly the same.

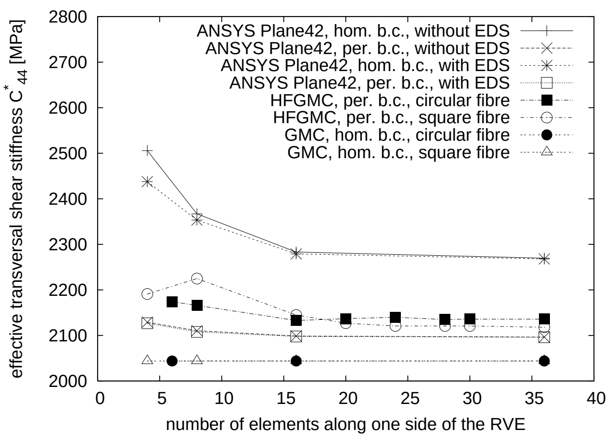

Fig. 2.2-4: Effective transverse stiffness C^*_{44} obtained by different micromechanical approaches [22]

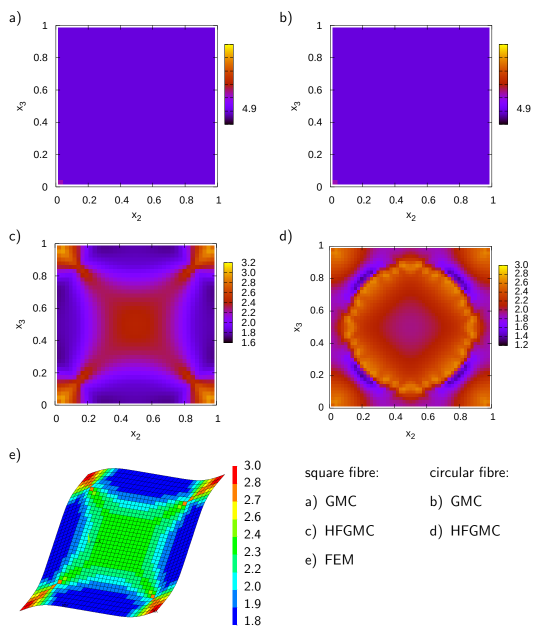

Fig. 2.2-5: Predicted stress distribution σ_{23} in GPa for $\epsilon_{23} = 1$ [22]

In Tab. 2.2-1, the stiffness components obtained by the different homogenization methods are compared for a square fibre shape and a mesh of 36×36 elements. The stiffness values C^*_{22} and C^*_{44} of the finite element analysis with periodic boundary conditions and EDS-option are selected as reference values (100%). The small difference of HFGMC and FEM accentuate the accuracy and application of the cell method. The GMC predicts the lowest stiffness values and, hence, it has a slightly higher deviation to the FEM results. Nevertheless, the GMC produces results,

Tab. 2.2-1: Homogenization results of GMC, HFGM and FEM with square fibre for 36 × 36 elements [22]

Stiffness	HFGMC	FEM, periodic b.c. with EDS	FEM, periodic b.c. without EDS	GMC	FEM, hom. b.c. with EDS	FEM, hom. b.c. without EDS
C^*_{22} [MPa]	8716.0	8693.6	8694.8	8520.0	8739.8	8741.0
C^*_{22} [%]	100.3	100.0	≈100.0	98.0	100.5	100.5
C^*_{44} [MPa]	2118.0	2096.2	2096.5	2044.0	2268.0	2269.8
C^*_{44} [%]	101.0	100.0	≈100.0	97.5	108.2	108.2

which are sufficient for the most engineering applications and is characterized by its numerical efficiently [22].

3 High Fidelity Method of Cells with Cohesive Interface Damage

M. Schmerbauch, M. Donhauser, A. Matzenmiller

3.1 Spatial Discretization

The volume $V_{\text{RUC}} = 1 \cdot A_{\text{RUC}}$ of a RUC is spatially discretized in $1 \times N_\beta \times N_\gamma$ rectangular solid-subcells $\Omega^{(\beta,\gamma)}$, see Fig. 3.1-1, where $\mathbf{y} = (y_1, y_2, y_3)$ denotes the global Cartesian coordinate system of the micro structure. The variables N_β and N_γ describe the number of solid-subcells in each direction, β and γ are pointers addressing the subcell $\Omega^{(\beta,\gamma)}$. The dimensions of each subcell are given by $l_2^{(\beta)}$ (y_2-direction) and $l_3^{(\gamma)}$ (y_3-direction) whose sums yield the absolute dimensions of the RUC L_2 and L_3:

$$L_2 = \sum_{\beta=1}^{N_\beta} l_2^{(\beta)} \qquad\qquad L_3 = \sum_{\gamma=1}^{N_\gamma} l_3^{(\gamma)} \; . \tag{3.1-1}$$

The displacement field in each subcell $\mathbf{u}^{(\beta,\gamma)} = \mathbf{u}^{(\beta,\gamma)}\left(\mathbf{x}, \mathbf{z}^{(\beta,\gamma)}\right)$ is approached by a constant macro part $\mathbf{u}^{0(\beta,\gamma)}(\mathbf{x}) = \boldsymbol{\varepsilon}^0(\mathbf{x})\mathbf{y}$ and a fluctuating one $\mathbf{u}'^{(\beta,\gamma)}(\mathbf{x}, \mathbf{z}^{(\beta,\gamma)})$

$$\mathbf{u}^{(\beta,\gamma)}\left(\mathbf{x}, \mathbf{z}^{(\beta,\gamma)}\right) = \mathbf{u}^{0(\beta,\gamma)}(\mathbf{x}) + \mathbf{u}'^{(\beta,\gamma)}(\mathbf{x}, \mathbf{z}^{(\beta,\gamma)}) \; , \tag{3.1-2}$$

where $\mathbf{x}$ stands for the position vector of a material point at the macro level, $\mathbf{z}^{(\beta\gamma)} = \left(z_1^{(\beta,\gamma)}, z_2^{(\beta,\gamma)}, z_3^{(\beta,\gamma)}\right)$ for the local Cartesian coordinate system defined in the center of subcell $\Omega^{(\beta,\gamma)}$ and $\boldsymbol{\varepsilon}^0$ for the macro strain. The fluctuating part $\mathbf{u}'^{(\beta,\gamma)}\left(\mathbf{x}, \mathbf{z}^{(\beta,\gamma)}\right)$ is a sum of Legendre-polynomial of zeroth,

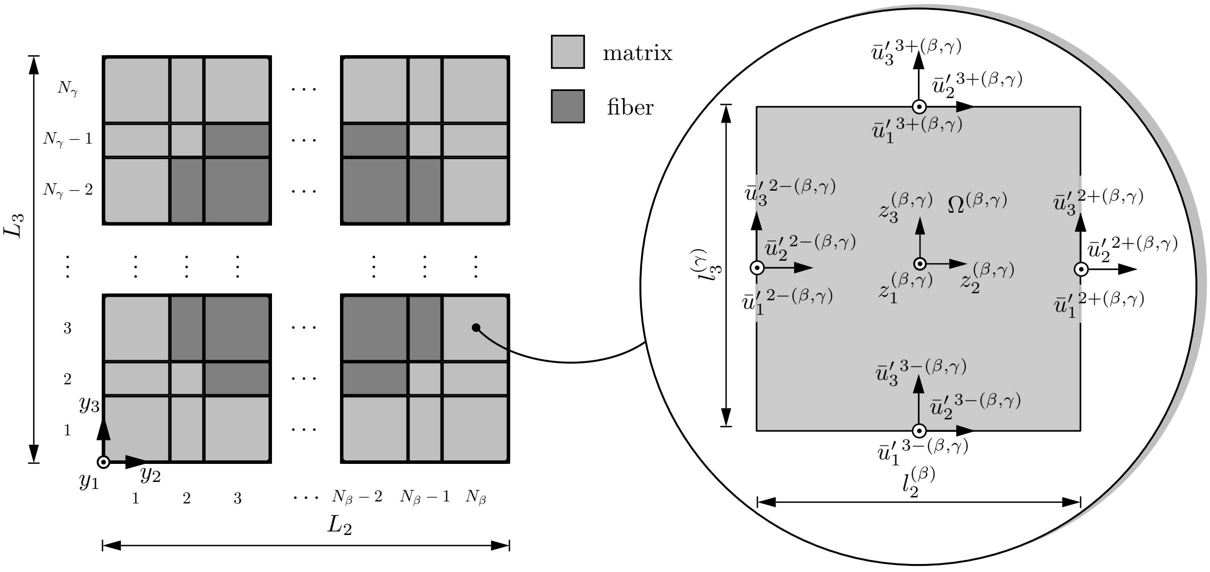

Fig. 3.1-1: Spatial dimensions, discretization and local degrees of freedom of RUC and subcell $\Omega^{(\beta,\gamma)}$

first and second order with unknown microvariables $\mathbf{W}_{(nm)}$, see [3].

$$\mathbf{u}'^{(\beta,\gamma)}\left(\mathbf{x},\mathbf{z}^{(\beta,\gamma)}\right) = \mathbf{W}^{(\beta,\gamma)}_{(00)} + z_2^{(\beta,\gamma)}\mathbf{W}^{(\beta,\gamma)}_{(10)} + z_3^{(\beta,\gamma)}\mathbf{W}^{(\beta,\gamma)}_{(01)} + \\ + \frac{1}{2}\left[3\left(z_2^{(\beta,\gamma)}\right)^2 - \frac{\left(l_2^{(\beta)}\right)^2}{4}\right]\mathbf{W}^{(\beta,\gamma)}_{(20)} + \frac{1}{2}\left[3\left(z_3^{(\beta,\gamma)}\right)^2 - \frac{\left(l_3^{(\gamma)}\right)^2}{4}\right]\mathbf{W}^{(\beta,\gamma)}_{(02)} \tag{3.1-3}$$

To represent damage and consequent cracks in the matrix phase and fiber/matrix debonding, interface subcells $\mathcal{S}^{n(j)}$ are inserted between adjacent solid-subcells, see Fig. 3.1-2, where j stands for the number of interface subcell j with its orientation in y_2-direction ($n = 2$) or in y_3-direction ($n = 3$). The dimensions of a interface-subcell $l_2^{n(j)}$ and $l_3^{n(j)}$ depend on the dimensions of the neighboring solid-subcells

$$l_3^{2(j)} = l_3\big|_{\Omega^{(\beta,\gamma)}} \qquad\qquad l_2^{3(j)} = l_2\big|_{\Omega^{(\beta,\gamma)}} \tag{3.1-4}$$
$$= l_3\big|_{\Omega^{(\beta-1,\gamma)}} \qquad\qquad = l_2\big|_{\Omega^{(\beta,\gamma-1)}} \ . \tag{3.1-5}$$

The microscopic strain field $\boldsymbol{\varepsilon}^{(\beta,\gamma)} = \boldsymbol{\varepsilon}^{(\beta,\gamma)}\left(\mathbf{x},\mathbf{z}^{(\beta,\gamma)}\right)$ of subcell $\Omega^{(\beta,\gamma)}$ results from the kinematic relations, see for instance [3]:

$$\varepsilon_{11}^{(\beta,\gamma)}\left(z_2^{(\beta,\gamma)}, z_3^{(\beta,\gamma)}\right) = \varepsilon_{11}^0 \tag{3.1-6}$$
$$\varepsilon_{22}^{(\beta,\gamma)}\left(z_2^{(\beta,\gamma)}, z_3^{(\beta,\gamma)}\right) = \varepsilon_{22}^0 + W^{(\beta,\gamma)}_{2(10)} + 3z_2^{(\beta,\gamma)}W^{(\beta,\gamma)}_{2(20)} \tag{3.1-7}$$
$$\varepsilon_{33}^{(\beta,\gamma)}\left(z_2^{(\beta,\gamma)}, z_3^{(\beta,\gamma)}\right) = \varepsilon_{33}^0 + W^{(\beta,\gamma)}_{3(01)} + 3z_3^{(\beta,\gamma)}W^{(\beta,\gamma)}_{3(02)} \tag{3.1-8}$$
$$\varepsilon_{12}^{(\beta,\gamma)}\left(z_2^{(\beta,\gamma)}, z_3^{(\beta,\gamma)}\right) = \varepsilon_{12}^0 + \frac{1}{2}\left[W^{(\beta,\gamma)}_{1(10)} + 3z_2^{(\beta,\gamma)}W^{(\beta,\gamma)}_{1(20)}\right] \tag{3.1-9}$$
$$\varepsilon_{13}^{(\beta,\gamma)}\left(z_2^{(\beta,\gamma)}, z_3^{(\beta,\gamma)}\right) = \varepsilon_{13}^0 + \frac{1}{2}\left[W^{(\beta,\gamma)}_{1(01)} + 3z_3^{(\beta,\gamma)}W^{(\beta,\gamma)}_{1(02)}\right] \tag{3.1-10}$$
$$\varepsilon_{23}^{(\beta,\gamma)}\left(z_2^{(\beta,\gamma)}, z_3^{(\beta,\gamma)}\right) = \varepsilon_{23}^0 + \frac{1}{2}\left[W^{(\beta,\gamma)}_{2(01)} + 3z_3^{(\beta,\gamma)}W^{(\beta,\gamma)}_{2(02)} + W^{(\beta,\gamma)}_{3(10)} + 3z_2^{(\beta,\gamma)}W^{(\beta,\gamma)}_{3(20)}\right] \ . \tag{3.1-11}$$

The averaged strain of each subcell is given by

$$\langle\varepsilon_{ij}^{(\beta,\gamma)}\rangle = \frac{1}{1\, l_2^{(\beta)}\, l_3^{(\gamma)}} \iiint\limits_V \varepsilon_{ij}^{(\beta,\gamma)}\, \mathrm{d}z_1^{(\beta,\gamma)}\, \mathrm{d}z_2^{(\beta,\gamma)}\, \mathrm{d}z_3^{(\beta,\gamma)} \ . \tag{3.1-12}$$

Using the strain definition of Eqs. (3.1-6) through (3.1-11), the components of the averaged strain in Eq. (3.1-12) become

$$\langle\varepsilon_{11}^{(\beta,\gamma)}\rangle = \varepsilon_{11}^0 \tag{3.1-13}$$
$$\langle\varepsilon_{22}^{(\beta,\gamma)}\rangle = \varepsilon_{22}^0 + W^{(\beta,\gamma)}_{2(10)} \tag{3.1-14}$$
$$\langle\varepsilon_{33}^{(\beta,\gamma)}\rangle = \varepsilon_{33}^0 + W^{(\beta,\gamma)}_{3(01)} \tag{3.1-15}$$
$$\langle\varepsilon_{12}^{(\beta,\gamma)}\rangle = \varepsilon_{12}^0 + \frac{1}{2}W^{(\beta,\gamma)}_{1(10)} \tag{3.1-16}$$
$$\langle\varepsilon_{13}^{(\beta,\gamma)}\rangle = \varepsilon_{13}^0 + \frac{1}{2}W^{(\beta,\gamma)}_{1(01)} \tag{3.1-17}$$
$$\langle\varepsilon_{23}^{(\beta,\gamma)}\rangle = \varepsilon_{23}^0 + \frac{1}{2}\left[W^{(\beta,\gamma)}_{2(01)} + W^{(\beta,\gamma)}_{3(10)}\right] \ . \tag{3.1-18}$$

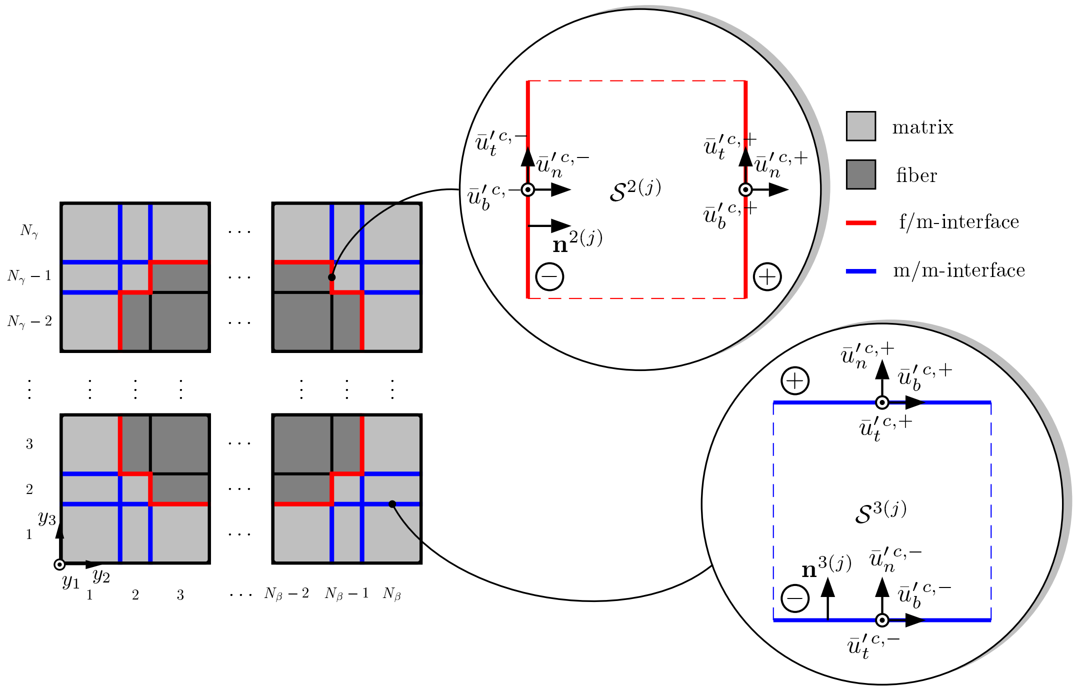

Fig. 3.1-2: Discretization of RUC with interface-subcells $\mathcal{S}^{n(j)}$ and their local degrees of freedom

Assuming linear-elastic material behaviour in each solid-subcell $\Omega^{(\beta,\gamma)}$

$$\boldsymbol{\sigma}^{(\beta,\gamma)} = \mathbf{C}^{(\beta,\gamma)} \boldsymbol{\varepsilon}^{(\beta,\gamma)} \ , \tag{3.1-19}$$

the averaged stress tensor is written as follows

$$\langle \boldsymbol{\sigma}^{(\beta,\gamma)} \rangle = \mathbf{C}^{(\beta,\gamma)} \langle \boldsymbol{\varepsilon}^{(\beta,\gamma)} \rangle \ , \tag{3.1-20}$$

where $\mathbf{C}^{(\beta,\gamma)}$ is the fourth order elastic stiffness tensor. The volume-averaged stress tensor $\langle \boldsymbol{\sigma} \rangle$ of the RUC results from the averaging process over the entire RUC:

$$\langle \boldsymbol{\sigma} \rangle = \frac{1}{1\, L_2\, L_3} \sum_{\beta=1}^{N_\beta} \sum_{\gamma=1}^{N_\gamma} \iiint_V \boldsymbol{\sigma}^{(\beta,\gamma)}(\mathbf{z}) \, \mathrm{d}z_1^{(\beta,\gamma)} \, \mathrm{d}z_2^{(\beta,\gamma)} \, \mathrm{d}z_3^{(\beta,\gamma)} \tag{3.1-21}$$

$$= \frac{1}{L_2\, L_3} \sum_{\beta=1}^{N_\beta} \sum_{\gamma=1}^{N_\gamma} l_2^{(\beta)} l_3^{(\gamma)} \langle \boldsymbol{\sigma}^{(\beta,\gamma)} \rangle \ . \tag{3.1-22}$$

3.2 Solid Subcells

At first, surface-averaged tractions $\bar{\mathbf{t}}^{n\pm(\beta,\gamma)}$ at the face $\partial\Omega^{n\pm(\beta,\gamma)}$ are established

$$\bar{\mathbf{t}}^{n\pm(\beta,\gamma)} = \frac{1}{l_n^{(\beta/\gamma)}} \int_{l_n^{(\beta/\gamma)}} \mathbf{t}^{n\pm(\beta,\gamma)}|_{\partial\Omega^{n\pm(\beta,\gamma)}} \, \mathrm{d}\tilde{l}_n^{(\beta/\gamma)} \tag{3.2-1}$$

by using Cauchy's theorem

$$\mathbf{t}^{n\pm(\beta,\gamma)} = \boldsymbol{\sigma}^{(\beta,\gamma)} \mathbf{n}^{n\pm(\beta,\gamma)} \tag{3.2-2}$$

and Hooke's law (3.1-19). In particular

$$\bar{\mathbf{t}}^{2\pm(\beta,\gamma)} = \frac{1}{l_3^{(\gamma)}} \int\limits_{-0.5\,l_3^{(\gamma)}}^{+0.5\,l_3^{(\gamma)}} \boldsymbol{\sigma}^{(\beta,\gamma)}(\pm 0.5\,l_2^{(\beta)}, z_3)\,\mathbf{n}^{2\pm}\,\mathrm{d}z_3^{(\beta,\gamma)} \quad \text{for } \mathbf{n} = \mathbf{e}_2 \tag{3.2-3}$$

and

$$\bar{\mathbf{t}}^{3\pm(\beta\gamma)} = \frac{1}{l_2^{(\beta)}} \int\limits_{-0.5\,l_2^{(\beta)}}^{+0.5\,l_2^{(\beta)}} \boldsymbol{\sigma}^{(\beta,\gamma)}(z_2, \pm 0.5\,l_2^{(\beta)})\,\mathbf{n}^{3\pm}\,\mathrm{d}z_2^{(\beta,\gamma)} \quad \text{for } \mathbf{n} = \mathbf{e}_3\ . \tag{3.2-4}$$

Using the constitutive equation (3.1-20) and Eqs. (3.1-13) - (3.1-18) the averaging in Eq. (3.2-3) and Eq. (3.2-4) leads to

$$\begin{Bmatrix} \vec{t}_1^{2+} \\ \vec{t}_1^{2-} \end{Bmatrix}^{(\beta,\gamma)} = C_{66}^{(\beta,\gamma)} \begin{bmatrix} 1 & \frac{3l_2^{(\beta)}}{2} \\ -1 & \frac{3l_2^{(\beta)}}{2} \end{bmatrix} \begin{Bmatrix} W_{1(10)} \\ W_{1(20)} \end{Bmatrix}^{(\beta,\gamma)} + 2C_{66}^{(\beta,\gamma)} \begin{Bmatrix} \varepsilon_{12}^0 \\ -\varepsilon_{12}^0 \end{Bmatrix} \tag{3.2-5}$$

$$\begin{Bmatrix} \vec{t}_2^{2+} \\ \vec{t}_2^{2-} \end{Bmatrix}^{(\beta,\gamma)} = C_{22}^{(\beta,\gamma)} \begin{bmatrix} 1 & \frac{3l_2^{(\beta)}}{2} \\ -1 & \frac{3l_2^{(\beta)}}{2} \end{bmatrix} \begin{Bmatrix} W_{2(10)} \\ W_{2(20)} \end{Bmatrix}^{(\beta,\gamma)} + C_{23}^{(\beta,\gamma)} \begin{Bmatrix} W_{3(01)} \\ -W_{3(01)} \end{Bmatrix}^{(\beta,\gamma)} + $$
$$+ \sum_{i=1}^{3} C_{i2}^{(\beta,\gamma)} \begin{Bmatrix} \varepsilon_{ii}^0 \\ -\varepsilon_{ii}^0 \end{Bmatrix}^{(\beta,\gamma)} \tag{3.2-6}$$

$$\begin{Bmatrix} \vec{t}_3^{2+} \\ \vec{t}_3^{2-} \end{Bmatrix}^{(\beta,\gamma)} = C_{44}^{(\beta,\gamma)} \begin{bmatrix} 1 & \frac{3l_2^{(\beta)}}{2} \\ -1 & \frac{3l_2^{(\beta)}}{2} \end{bmatrix} \begin{Bmatrix} W_{3(10)} \\ W_{3(20)} \end{Bmatrix}^{(\beta,\gamma)} + C_{44}^{(\beta,\gamma)} \begin{Bmatrix} W_{2(01)} \\ -W_{2(01)} \end{Bmatrix}^{(\beta,\gamma)} + $$

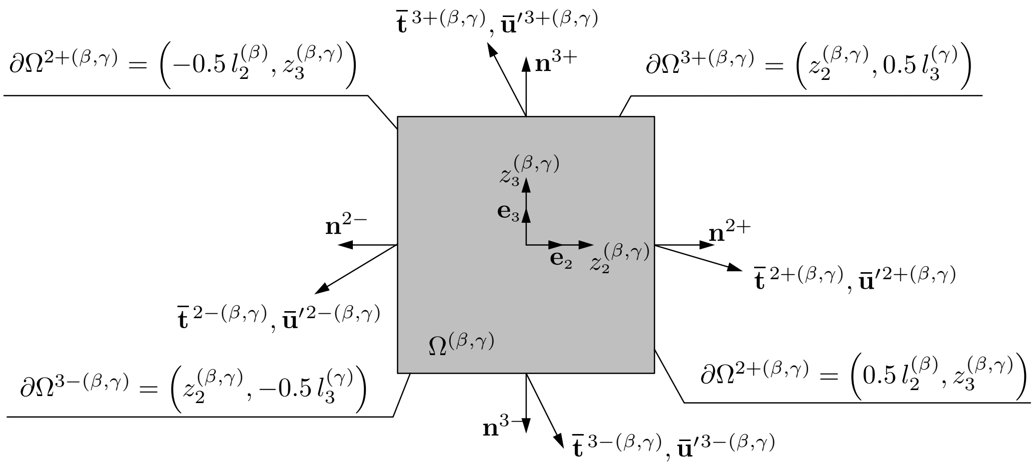

Fig. 3.2-1: Surface-averaged displacements $\bar{\mathbf{u}}'^{\mathbf{n}\pm(\beta,\gamma)}$, tractions $\bar{\mathbf{t}}^{n\pm(\beta,\gamma)}$ and surface normal $\mathbf{n}^{n\pm}$ at surfaces $\partial\Omega^{2+}$, $\partial\Omega^{2-}$, $\partial\Omega^{3+}$ und $\partial\Omega^{3-}$ of subcell $\Omega^{(\beta,\gamma)}$

$$+ 2C_{44}^{(\beta,\gamma)} \begin{Bmatrix} \varepsilon_{23}^{0} \\ -\varepsilon_{23}^{0} \end{Bmatrix} \tag{3.2-7}$$

$$\begin{Bmatrix} \bar{t}_1^{3+} \\ \bar{t}_1^{3-} \end{Bmatrix}^{(\beta,\gamma)} = C_{55}^{(\beta,\gamma)} \begin{bmatrix} 1 & \dfrac{3l_3^{(\gamma)}}{2} \\ -1 & \dfrac{3l_3^{(\gamma)}}{2} \end{bmatrix} \begin{Bmatrix} W_{1(01)} \\ W_{1(02)} \end{Bmatrix}^{(\beta,\gamma)} + 2C_{55}^{(\beta,\gamma)} \begin{Bmatrix} \varepsilon_{13}^{0} \\ -\varepsilon_{13}^{0} \end{Bmatrix} \tag{3.2-8}$$

$$\begin{Bmatrix} \bar{t}_2^{3+} \\ \bar{t}_2^{3-} \end{Bmatrix}^{(\beta,\gamma)} = C_{44}^{(\beta,\gamma)} \begin{bmatrix} 1 & \dfrac{3l_3^{(\gamma)}}{2} \\ -1 & \dfrac{3l_3^{(\gamma)}}{2} \end{bmatrix} \begin{Bmatrix} W_{2(01)} \\ W_{2(02)} \end{Bmatrix}^{(\beta,\gamma)} + C_{44}^{(\beta,\gamma)} \begin{Bmatrix} W_{3(10)} \\ -W_{3(10)} \end{Bmatrix}^{(\beta,\gamma)} +$$

$$+ 2C_{44}^{(\beta,\gamma)} \begin{Bmatrix} \varepsilon_{23}^{0} \\ -\varepsilon_{23}^{0} \end{Bmatrix} \tag{3.2-9}$$

$$\begin{Bmatrix} \bar{t}_3^{3+} \\ \bar{t}_3^{3-} \end{Bmatrix}^{(\beta,\gamma)} = C_{33}^{(\beta,\gamma)} \begin{bmatrix} 1 & \dfrac{3l_3^{(\gamma)}}{2} \\ -1 & \dfrac{3l_3^{(\gamma)}}{2} \end{bmatrix} \begin{Bmatrix} W_{3(01)} \\ W_{3(02)} \end{Bmatrix}^{(\beta,\gamma)} + C_{23}^{(\beta,\gamma)} \begin{Bmatrix} W_{2(10)} \\ -W_{2(10)} \end{Bmatrix}^{(\beta,\gamma)} +$$

$$+ \sum_{i=1}^{3} C_{i3}^{(\beta,\gamma)} \begin{Bmatrix} \varepsilon_{ii}^{0} \\ -\varepsilon_{ii}^{0} \end{Bmatrix} . \tag{3.2-10}$$

The fluctuating displacements $\mathbf{u}'^{(\beta,\gamma)}$ are averaged in the same way as the surface-averaged tractions in a next step at each face $\partial\Omega^{n\pm(\beta,\gamma)}$

$$\bar{\mathbf{u}}'^{n\pm(\beta,\gamma)} = \frac{1}{l_n^{(\beta/\gamma)}} \int\limits_{l_n^{(\beta/\gamma)}} \mathbf{u}'^{(\beta,\gamma)}\big|_{\partial\Omega^{n\pm}} \, \mathrm{d}\tilde{l}_n^{(\beta/\gamma)} , \tag{3.2-11}$$

in particular

$$\bar{\mathbf{u}}^{2\pm(\beta,\gamma)} = \frac{1}{l_3^{(\gamma)}} \int\limits_{-0.5\,l_3^{(\gamma)}}^{+0.5\,l_3^{(\gamma)}} \mathbf{u}'^{(\beta,\gamma)}(\pm 0.5\,l_2^{(\beta)}, z_3)\, \mathrm{d}z_3^{(\beta,\gamma)} \quad \text{for } \mathbf{n} = \mathbf{e}_2 \tag{3.2-12}$$

and

$$\bar{\mathbf{u}}'^{3\pm(\beta,\gamma)} = \frac{1}{l_2^{(\beta)}} \int\limits_{-0.5\,l_2^{(\beta)}}^{+0.5\,l_2^{(\beta)}} \mathbf{u}'^{(\beta,\gamma)}(z_2, \pm 0.5\,l_2^{(\beta)})\, \mathrm{d}z_2^{(\beta,\gamma)} \quad \text{for } \mathbf{n} = \mathbf{e}_3 \; . \tag{3.2-13}$$

The averaging process in Eqs. (3.2-12) and (3.2-13) yields

$$\begin{Bmatrix} \bar{u}_1^{2+} \\ \bar{u}_1^{2-} \end{Bmatrix}^{(\beta,\gamma)} = \begin{bmatrix} \dfrac{l_2^{(\beta)}}{2} & \dfrac{\left(l_2^{(\beta)}\right)^2}{4} \\ -\dfrac{l_2^{(\beta)}}{2} & \dfrac{\left(l_2^{(\beta)}\right)^2}{4} \end{bmatrix} \begin{Bmatrix} W_{1(10)} \\ W_{1(20)} \end{Bmatrix}^{(\beta,\gamma)} + \begin{Bmatrix} W_{1(00)} \\ W_{1(00)} \end{Bmatrix}^{(\beta,\gamma)} \tag{3.2-14}$$

$$\begin{Bmatrix} \bar{u}_2^{2+} \\ \bar{u}_2^{2-} \end{Bmatrix}^{(\beta,\gamma)} = \begin{bmatrix} \frac{l_2^{(\beta)}}{2} & \frac{\left(l_2^{(\beta)}\right)^2}{4} \\ -\frac{l_2^{(\beta)}}{2} & \frac{\left(l_2^{(\beta)}\right)^2}{4} \end{bmatrix} \begin{Bmatrix} W_{2(10)} \\ W_{2(20)} \end{Bmatrix}^{(\beta,\gamma)} + \begin{Bmatrix} W_{2(00)} \\ W_{2(00)} \end{Bmatrix}^{(\beta,\gamma)} \tag{3.2-15}$$

$$\begin{Bmatrix} \bar{u}_3^{2+} \\ \bar{u}_3^{2-} \end{Bmatrix}^{(\beta,\gamma)} = \begin{bmatrix} \frac{l_2^{(\beta)}}{2} & \frac{\left(l_2^{(\beta)}\right)^2}{4} \\ -\frac{l_2^{(\beta)}}{2} & \frac{\left(l_2^{(\beta)}\right)^2}{4} \end{bmatrix} \begin{Bmatrix} W_{3(10)} \\ W_{3(20)} \end{Bmatrix}^{(\beta,\gamma)} + \begin{Bmatrix} W_{3(00)} \\ W_{3(00)} \end{Bmatrix}^{(\beta,\gamma)} \tag{3.2-16}$$

$$\begin{Bmatrix} \bar{u}_1^{3+} \\ \bar{u}_1^{3-} \end{Bmatrix}^{(\beta,\gamma)} = \begin{bmatrix} \frac{l_3^{(\gamma)}}{2} & \frac{\left(l_3^{(\gamma)}\right)^2}{4} \\ -\frac{l_3^{(\gamma)}}{2} & \frac{\left(l_3^{(\gamma)}\right)^2}{4} \end{bmatrix} \begin{Bmatrix} W_{1(01)} \\ W_{1(02)} \end{Bmatrix}^{(\beta,\gamma)} + \begin{Bmatrix} W_{1(00)} \\ W_{1(00)} \end{Bmatrix}^{(\beta,\gamma)} \tag{3.2-17}$$

$$\begin{Bmatrix} \bar{u}_2^{3+} \\ \bar{u}_2^{3-} \end{Bmatrix}^{(\beta,\gamma)} = \begin{bmatrix} \frac{l_3^{(\gamma)}}{2} & \frac{\left(l_3^{(\gamma)}\right)^2}{4} \\ -\frac{l_3^{(\gamma)}}{2} & \frac{\left(l_3^{(\gamma)}\right)^2}{4} \end{bmatrix} \begin{Bmatrix} W_{2(01)} \\ W_{2(02)} \end{Bmatrix}^{(\beta,\gamma)} + \begin{Bmatrix} W_{2(00)} \\ W_{2(00)} \end{Bmatrix}^{(\beta,\gamma)} \tag{3.2-18}$$

$$\begin{Bmatrix} \bar{u}_3^{3+} \\ \bar{u}_3^{3-} \end{Bmatrix}^{(\beta,\gamma)} = \begin{bmatrix} \frac{l_3^{(\gamma)}}{2} & \frac{\left(l_3^{(\gamma)}\right)^2}{4} \\ -\frac{l_3^{(\gamma)}}{2} & \frac{\left(l_3^{(\gamma)}\right)^2}{4} \end{bmatrix} \begin{Bmatrix} W_{3(01)} \\ W_{3(02)} \end{Bmatrix}^{(\beta,\gamma)} + \begin{Bmatrix} W_{3(00)} \\ W_{3(00)} \end{Bmatrix}^{(\beta,\gamma)} \tag{3.2-19}$$

by using the fluctuating displacement approach (3.1-3). In order to link the surface-averaged fluctuating displacements in Eqs. (3.2-14) through (3.2-19) to the surface-averaged tractions in Eqs. (3.2-5) through (3.2-10), Eqs. (3.2-14) through (3.2-19) are solved for the micro variables $\mathbf{W}_{(nm)}$ with $n \neq m$

$$\begin{Bmatrix} W_{1(10)} \\ W_{1(20)} \end{Bmatrix}^{(\beta,\gamma)} = \begin{bmatrix} \frac{1}{l_2^{(\beta)}} & -\frac{1}{l_2^{(\beta)}} \\ \frac{2}{\left(l_2^{(\beta)}\right)^2} & \frac{2}{\left(l_2^{(\beta)}\right)^2} \end{bmatrix} \begin{Bmatrix} \bar{u}_1^{2+} \\ \bar{u}_1^{2-} \end{Bmatrix}^{(\beta,\gamma)} - \frac{4}{\left(l_2^{(\beta)}\right)^2} \begin{Bmatrix} 0 \\ W_{1(00)} \end{Bmatrix}^{(\beta,\gamma)} \tag{3.2-20}$$

$$\begin{Bmatrix} W_{2(10)} \\ W_{2(20)} \end{Bmatrix}^{(\beta,\gamma)} = \begin{bmatrix} \frac{1}{l_2^{(\beta)}} & -\frac{1}{l_2^{(\beta)}} \\ \frac{2}{\left(l_2^{(\beta)}\right)^2} & \frac{2}{\left(l_2^{(\beta)}\right)^2} \end{bmatrix} \begin{Bmatrix} \bar{u}_2^{2+} \\ \bar{u}_2^{2-} \end{Bmatrix}^{(\beta,\gamma)} - \frac{4}{\left(l_2^{(\beta)}\right)^2} \begin{Bmatrix} 0 \\ W_{2(00)} \end{Bmatrix}^{(\beta,\gamma)} \tag{3.2-21}$$

$$\begin{Bmatrix} W_{3(10)} \\ W_{3(20)} \end{Bmatrix}^{(\beta,\gamma)} = \begin{bmatrix} \frac{1}{l_2^{(\beta)}} & -\frac{1}{l_2^{(\beta)}} \\ \frac{2}{\left(l_2^{(\beta)}\right)^2} & \frac{2}{\left(l_2^{(\beta)}\right)^2} \end{bmatrix} \begin{Bmatrix} \bar{u}_3^{2+} \\ \bar{u}_3^{2-} \end{Bmatrix}^{(\beta,\gamma)} - \frac{4}{\left(l_2^{(\beta)}\right)^2} \begin{Bmatrix} 0 \\ W_{3(00)} \end{Bmatrix}^{(\beta,\gamma)} \tag{3.2-22}$$

$$\begin{Bmatrix} W_{1(01)} \\ W_{1(02)} \end{Bmatrix}^{(\beta,\gamma)} = \begin{bmatrix} \dfrac{1}{l_3^{(\gamma)}} & -\dfrac{1}{l_3^{(\gamma)}} \\ \dfrac{2}{\left(l_3^{(\gamma)}\right)^2} & \dfrac{2}{\left(l_3^{(\gamma)}\right)^2} \end{bmatrix} \begin{Bmatrix} \bar{u}_1^{3+} \\ \bar{u}_1^{3-} \end{Bmatrix}^{(\beta,\gamma)} - \frac{4}{\left(l_3^{(\gamma)}\right)^2} \begin{Bmatrix} 0 \\ W_{1(00)} \end{Bmatrix}^{(\beta,\gamma)} \tag{3.2-23}$$

$$\begin{Bmatrix} W_{2(01)} \\ W_{2(02)} \end{Bmatrix}^{(\beta,\gamma)} = \begin{bmatrix} \dfrac{1}{l_3^{(\gamma)}} & -\dfrac{1}{l_3^{(\gamma)}} \\ \dfrac{2}{\left(l_3^{(\gamma)}\right)^2} & \dfrac{2}{\left(l_3^{(\gamma)}\right)^2} \end{bmatrix} \begin{Bmatrix} \bar{u}_2^{3+} \\ \bar{u}_2^{3-} \end{Bmatrix}^{(\beta,\gamma)} - \frac{4}{\left(l_3^{(\gamma)}\right)^2} \begin{Bmatrix} 0 \\ W_{2(00)} \end{Bmatrix}^{(\beta,\gamma)} \tag{3.2-24}$$

$$\begin{Bmatrix} W_{3(01)} \\ W_{3(02)} \end{Bmatrix}^{(\beta,\gamma)} = \begin{bmatrix} \dfrac{1}{l_3^{(\gamma)}} & -\dfrac{1}{l_3^{(\gamma)}} \\ \dfrac{2}{\left(l_3^{(\gamma)}\right)^2} & \dfrac{2}{\left(l_3^{(\gamma)}\right)^2} \end{bmatrix} \begin{Bmatrix} \bar{u}_3^{3+} \\ \bar{u}_3^{3-} \end{Bmatrix}^{(\beta,\gamma)} - \frac{4}{\left(l_3^{(\gamma)}\right)^2} \begin{Bmatrix} 0 \\ W_{3(00)} \end{Bmatrix}^{(\beta,\gamma)} . \tag{3.2-25}$$

The missing three equations for the zeroth-order micro variables $\mathbf{W}_{(00)}$ are determined by the linear momentum in absence of volume forces. The static equilibrium is satisfied on average for each subcell volume $\Omega^{(\beta,\gamma)}$

$$\int\limits_{-0.5\,l_3^{(\gamma)}}^{+0.5\,l_3^{(\gamma)}} \int\limits_{-0.5\,l_2^{(\beta)}}^{+0.5\,l_2^{(\beta)}} \int\limits_{0}^{1} (\boldsymbol{\nabla}\cdot\boldsymbol{\sigma})^{(\beta,\gamma)}\, \mathrm{d}z_1^{(\beta,\gamma)}\, \mathrm{d}z_2^{(\beta,\gamma)}\, \mathrm{d}z_3^{(\beta,\gamma)} = 0\ . \tag{3.2-26}$$

Replacing the stress divergence $(\boldsymbol{\nabla}\cdot\boldsymbol{\sigma})^{(\beta,\gamma)}$ by the constitutive Eq. (3.1-19) and the derivative of the subcell strains $\boldsymbol{\varepsilon}^{(\beta\gamma)}$ by the micro variables $\mathbf{W}_{(nm)}$ with $n \neq m$ of Eqs. (3.2-20) through (3.2-25), the integration of Eq. (3.2-26) provides the unknown micro variables:

$$W_{1(00)}^{(\beta,\gamma)} = \frac{C_{66}^{(\beta,\gamma)}}{2\bar{C}_{11}^{(\beta,\gamma)}}\left(\bar{u}_1^{2+(\beta,\gamma)} + \bar{u}_1^{2-(\beta,\gamma)}\right) + \frac{\left(l_2^{(\beta)}\right)^2 C_{55}^{(\beta,\gamma)}}{2\left(l_3^{(\gamma)}\right)^2 \bar{C}_{11}^{(\beta,\gamma)}}\left(\bar{u}_1^{3+(\beta,\gamma)} + \bar{u}_1^{3-(\beta,\gamma)}\right) \tag{3.2-27}$$

$$W_{2(00)}^{(\beta,\gamma)} = \frac{C_{22}^{(\beta,\gamma)}}{2\bar{C}_{22}^{(\beta,\gamma)}}\left(\bar{u}_2^{2+(\beta,\gamma)} + \bar{u}_2^{2-(\beta,\gamma)}\right) + \frac{\left(l_2^{(\beta)}\right)^2 C_{44}^{(\beta,\gamma)}}{2\left(l_3^{(\gamma)}\right)^2 \bar{C}_{22}^{(\beta,\gamma)}}\left(\bar{u}_2^{3+(\beta,\gamma)} + \bar{u}_2^{3-(\beta,\gamma)}\right) \tag{3.2-28}$$

$$W_{3(00)}^{(\beta,\gamma)} = \frac{\left(l_3^{(\gamma)}\right)^2 C_{44}^{(\beta,\gamma)}}{2\left(l_2^{(\beta)}\right)^2 \bar{C}_{33}^{(\beta,\gamma)}}\left(\bar{u}_3^{2+(\beta,\gamma)} + \bar{u}_3^{2-(\beta,\gamma)}\right) + \frac{C_{33}^{(\beta,\gamma)}}{2\bar{C}_{33}^{(\beta,\gamma)}}\left(\bar{u}_3^{3+(\beta,\gamma)} + \bar{u}_3^{3-(\beta,\gamma)}\right) \tag{3.2-29}$$

with the abbreviations

$$\bar{C}_{11}^{(\beta,\gamma)} = C_{66}^{(\beta,\gamma)} + C_{55}^{(\beta,\gamma)}\left(\frac{l_2^{(\beta)}}{l_3^{(\gamma)}}\right)^2 \tag{3.2-30}$$

$$\bar{C}_{22}^{(\beta,\gamma)} = C_{22}^{(\beta,\gamma)} + C_{44}^{(\beta,\gamma)}\left(\frac{l_2^{(\beta)}}{l_3^{(\gamma)}}\right)^2 \tag{3.2-31}$$

$$\bar{C}_{33}^{(\beta,\gamma)} = C_{33}^{(\beta,\gamma)} + C_{44}^{(\beta,\gamma)}\left(\frac{l_3^{(\gamma)}}{l_2^{(\beta)}}\right)^2 . \tag{3.2-32}$$

Using the equation of the micro variables (3.2-20) through (3.2-25) and (3.2-27) through (3.2-29) in Eqs. (3.2-5) through (3.2-10), a relation between the surface-averaged tractions $\bar{\mathbf{t}}^{n\pm(\beta,\gamma)}$ and the surface-averaged fluctuating displacements $\bar{\mathbf{u}}'^{n\pm(\beta,\gamma)}$ is established, see [5]:

$$\begin{Bmatrix} \bar{t}_1^{2+} \\ \bar{t}_1^{2-} \\ \bar{t}_2^{2+} \\ \bar{t}_2^{2-} \\ \bar{t}_3^{2+} \\ \bar{t}_3^{2-} \\ \bar{t}_1^{3+} \\ \bar{t}_1^{3-} \\ \bar{t}_2^{3+} \\ \bar{t}_2^{3-} \\ \bar{t}_3^{3+} \\ \bar{t}_3^{3-} \end{Bmatrix}^{(\beta\gamma)} = \begin{bmatrix} K_{1,1} & K_{1,2} & 0 & 0 & 0 & 0 & K_{1,7} & K_{1,8} & 0 & 0 & 0 & 0 \\ K_{2,1} & K_{2,2} & 0 & 0 & 0 & 0 & K_{2,7} & K_{2,8} & 0 & 0 & 0 & 0 \\ 0 & 0 & K_{3,3} & K_{3,4} & 0 & 0 & 0 & 0 & K_{3,9} & K_{3,10} & K_{3,11} & K_{3,12} \\ 0 & 0 & K_{4,3} & K_{4,4} & 0 & 0 & 0 & 0 & K_{4,9} & K_{4,10} & K_{4,11} & K_{4,12} \\ 0 & 0 & 0 & 0 & K_{5,5} & K_{5,6} & 0 & 0 & K_{5,9} & K_{5,10} & K_{5,11} & K_{5,12} \\ 0 & 0 & 0 & 0 & K_{6,5} & K_{6,6} & 0 & 0 & K_{6,9} & K_{6,10} & K_{6,11} & K_{6,12} \\ K_{7,1} & K_{7,2} & 0 & 0 & 0 & 0 & K_{7,7} & K_{7,8} & 0 & 0 & 0 & 0 \\ K_{8,1} & K_{8,2} & 0 & 0 & 0 & 0 & K_{8,7} & K_{8,8} & 0 & 0 & 0 & 0 \\ 0 & 0 & K_{9,3} & K_{9,4} & K_{9,5} & K_{9,6} & 0 & 0 & K_{9,9} & K_{9,10} & 0 & 0 \\ 0 & 0 & K_{10,3} & K_{10,4} & K_{10,5} & K_{10,6} & 0 & 0 & K_{10,9} & K_{10,10} & 0 & 0 \\ 0 & 0 & K_{11,3} & K_{11,4} & K_{11,5} & K_{11,6} & 0 & 0 & 0 & 0 & K_{11,11} & K_{11,12} \\ 0 & 0 & K_{12,3} & K_{12,4} & K_{12,5} & K_{12,6} & 0 & 0 & 0 & 0 & K_{12,11} & K_{12,12} \end{bmatrix}^{(\beta\gamma)} \begin{Bmatrix} \bar{u}_1'^{2+} \\ \bar{u}_1'^{2-} \\ \bar{u}_2'^{2+} \\ \bar{u}_2'^{2-} \\ \bar{u}_3'^{2+} \\ \bar{u}_3'^{2-} \\ \bar{u}_1'^{3+} \\ \bar{u}_1'^{3-} \\ \bar{u}_2'^{3+} \\ \bar{u}_2'^{3-} \\ \bar{u}_3'^{3+} \\ \bar{u}_3'^{3-} \end{Bmatrix}^{(\beta\gamma)} +$$

$$+ \begin{bmatrix} 0 & 0 & 0 & 0 & D_{15} & 0 \\ 0 & 0 & 0 & 0 & D_{25} & 0 \\ D_{31} & D_{32} & D_{33} & 0 & 0 & 0 \\ D_{41} & D_{42} & D_{43} & 0 & 0 & 0 \\ 0 & 0 & 0 & D_{54} & 0 & 0 \\ 0 & 0 & 0 & D_{64} & 0 & 0 \\ 0 & 0 & 0 & 0 & 0 & D_{76} \\ 0 & 0 & 0 & 0 & 0 & D_{86} \\ 0 & 0 & 0 & D_{94} & 0 & 0 \\ 0 & 0 & 0 & D_{10,4} & 0 & 0 \\ D_{11,1} & D_{11,2} & D_{11,3} & 0 & 0 & 0 \\ D_{12,1} & D_{12,2} & D_{12,3} & 0 & 0 & 0 \end{bmatrix}^{(\beta\gamma)} \begin{Bmatrix} \varepsilon_{11}^0 \\ \varepsilon_{22}^0 \\ \varepsilon_{33}^0 \\ \varepsilon_{23}^0 \\ \varepsilon_{12}^0 \\ \varepsilon_{13}^0 \end{Bmatrix} , \tag{3.2-33}$$

which is briefly written to

$$\bar{\mathbf{t}}^{(\beta,\gamma)} = \mathbf{K}^{(\beta,\gamma)} \bar{\mathbf{u}}'^{(\beta,\gamma)} + \mathbf{D}^{(\beta,\gamma)} \boldsymbol{\varepsilon}^0 , \tag{3.2-34}$$

where $\mathbf{K}^{(\beta,\gamma)}$ denotes the solid-subcell stiffness matrix comprising material properties and subcell dimensions, as well as $\mathbf{D}^{(\beta,\gamma)}$ is a matrix with elastic stiffness components $\mathrm{C}_{ij}^{(\beta,\gamma)}$. Both matrices, $\mathbf{K}^{(\beta,\gamma)}$ and $\mathbf{D}^{(\beta,\gamma)}$, are specified in the Appendix A. The matrix $\mathbf{K}^{(\beta,\gamma)}$ is in case of a rectangular solid-subcells a non-symmetric matrix. Only for the special case $l_2^{(\beta)} = l_3^{(\gamma)}$, i. e. in case of quadratic solid-subcells $\Omega^{(\beta,\gamma)}$, $\mathbf{K}^{(\beta,\gamma)}$ is symmetric.

3.3 Interface Subcells

A interface-subcell shares its faces with the adjacent solid-subcells:

$$\Gamma^{-2(j)} = \partial\Omega^{2+(\beta,\gamma)} \qquad \Gamma^{+2(j)} = \partial\Omega^{2-(\beta+1,\gamma)} \qquad \text{for } \mathbf{n} = \mathbf{e}_2 \tag{3.3-1}$$

$$\Gamma^{-3(j)} = \partial\Omega^{3+(\beta,\gamma)} \qquad \Gamma^{+3(j)} = \partial\Omega^{3-(\beta,\gamma+1)} \qquad \text{for } \mathbf{n} = \mathbf{e}_3 \ , \tag{3.3-2}$$

where the unit vector of an interface $\mathcal{S}^{n(j)}$ points from the negative crack face $\Gamma^{-n(j)}$ to the positive face $\Gamma^{+n(j)}$, see Fig. 3.1-2. The traction continuity in an averaged sense is forced between the cohesive traction $\bar{\mathbf{t}}^{\,\mathrm{I},\pm}$

$$\bar{\mathbf{t}}^{\,\mathrm{I},+} + \bar{\mathbf{t}}^{\,\mathrm{I},-} = 0 \qquad \begin{Bmatrix} \bar{t}_n^{\mathrm{I},+} \\ \bar{t}_t^{\mathrm{I},+} \\ \bar{t}_b^{\mathrm{I},+} \end{Bmatrix} + \begin{Bmatrix} \bar{t}_n^{\mathrm{I},-} \\ \bar{t}_t^{\mathrm{I},-} \\ \bar{t}_b^{\mathrm{I},-} \end{Bmatrix} = 0 \ . \tag{3.3-3}$$

The traction-separation-law is employed with surface-averaged quantities

$$\bar{\mathbf{t}}^{\,\mathrm{I}} = \mathbf{\Omega} \cdot \bar{\mathbf{\Delta}}'^{\,\mathrm{I}} \ , \tag{3.3-4}$$

where $\mathbf{\Omega}$ is the stiffness matrix of the interface and $\bar{\mathbf{\Delta}}'^{\,\mathrm{I}}$ is the local surface-averaged displacement jump vector

$$\bar{\mathbf{\Delta}}'^{\,\mathrm{I}} = \bar{\mathbf{u}}'^{\,\mathrm{I},+} - \bar{\mathbf{u}}'^{\,\mathrm{I},-} \ . \tag{3.3-5}$$

The local displacements of the interface $\bar{\mathbf{u}}'^{\,\mathrm{I},+}$ and $\bar{\mathbf{u}}'^{\,\mathrm{I},-}$ are shared with the adjacent solid-subcells. The traction-separation law is rewritten for the positive and negative face, satisfying the traction continuity (3.3-3)

$$\bar{\mathbf{t}}^{\,\mathrm{I},+} = -\mathbf{\Omega} \cdot \left(\bar{\mathbf{u}}'^{\,\mathrm{I},+} - \bar{\mathbf{u}}'^{\,\mathrm{I},-}\right) \qquad \bar{\mathbf{t}}^{\,\mathrm{I},-} = \mathbf{\Omega} \cdot \left(\bar{\mathbf{u}}'^{\,\mathrm{I},+} - \bar{\mathbf{u}}'^{\,\mathrm{I},-}\right) \ . \tag{3.3-6}$$

The tractions in Eqs. $(3.3\text{-}6)_1$ and $(3.3\text{-}6)_2$ are sorted in vector-matrix notation whereby the following interface system of equations is obtained:

$$\begin{Bmatrix} \bar{t}_n^{\mathrm{I},+} \\ \bar{t}_t^{\mathrm{I},+} \\ \bar{t}_b^{\mathrm{I},+} \\ \bar{t}_n^{\mathrm{I},-} \\ \bar{t}_t^{\mathrm{I},-} \\ \bar{t}_b^{\mathrm{I},-} \end{Bmatrix}^{n(j)} = \begin{bmatrix} -\Omega_{nn} & 0 & 0 & \Omega_{nn} & 0 & 0 \\ 0 & -\Omega_{tt} & 0 & 0 & \Omega_{tt} & 0 \\ 0 & 0 & -\Omega_{bb} & 0 & 0 & \Omega_{bb} \\ \Omega_{nn} & 0 & 0 & -\Omega_{nn} & 0 & 0 \\ 0 & \Omega_{tt} & 0 & 0 & -\Omega_{tt} & 0 \\ 0 & 0 & \Omega_{bb} & 0 & 0 & -\Omega_{bb} \end{bmatrix}^{n(j)} \begin{Bmatrix} \bar{u}_n'^{\,\mathrm{I},+} \\ \bar{u}_t'^{\,\mathrm{I},+} \\ \bar{u}_b'^{\,\mathrm{I},+} \\ \bar{u}_n'^{\,\mathrm{I},-} \\ \bar{u}_t'^{\,\mathrm{I},-} \\ \bar{u}_b'^{\,\mathrm{I},-} \end{Bmatrix}^{n(j)} , \tag{3.3-7}$$

which is briefly written to

$$\bar{\mathbf{t}}^{\mathrm{I},n(j)} = \mathbf{I}^{n(j)} \bar{\mathbf{u}}'^{\mathrm{I},n(j)} \ . \tag{3.3-8}$$

The notation $\mathbf{I}$ for the matrix in Eq. (3.3-7) must be chosen because it must differ from the matrix $\mathbf{\Omega}$ of the traction-separation law and its components, hence:

$$\begin{Bmatrix} \bar{t}_n^{\mathrm{I},+} \\ \bar{t}_t^{\mathrm{I},+} \\ \bar{t}_b^{\mathrm{I},+} \\ \bar{t}_n^{\mathrm{I},-} \\ \bar{t}_t^{\mathrm{I},-} \\ \bar{t}_b^{\mathrm{I},-} \end{Bmatrix}^{n(j)} = \begin{bmatrix} I_{11} & 0 & 0 & I_{14} & 0 & 0 \\ 0 & I_{22} & 0 & 0 & I_{25} & 0 \\ 0 & 0 & I_{33} & 0 & 0 & I_{36} \\ I_{41} & 0 & 0 & I_{44} & 0 & 0 \\ 0 & I_{52} & 0 & 0 & I_{55} & 0 \\ 0 & 0 & I_{63} & 0 & 0 & I_{66} \end{bmatrix}^{n(j)} \begin{Bmatrix} \bar{u}_n^{\mathrm{I},+} \\ \bar{u}_t^{\mathrm{I},+} \\ \bar{u}_b^{\mathrm{I},+} \\ \bar{u}_n^{\mathrm{I},-} \\ \bar{u}_t^{\mathrm{I},-} \\ \bar{u}_b^{\mathrm{I},-} \end{Bmatrix}^{n(j)} \tag{3.3-9}$$

with the components

$$I_{11} = I_{44} = -I_{14} = -I_{41} = -\Omega_{nn} \tag{3.3-10}$$

$$I_{22} = I_{55} = -I_{25} = -I_{52} = -\Omega_{tt} \tag{3.3-11}$$

$$I_{33} = I_{66} = -I_{36} = -I_{63} = -\Omega_{bb} \ . \tag{3.3-12}$$

3.4 Constitutive Equations

3.4.1 Traction-Separation-Model by Chaboche

The traction-separation-law proposed by Chaboche [11] links the tractions $\mathbf{t}$ to the local displacement jump $\mathbf{\Delta}$ by a stiffness tensor $\mathbf{\Omega}$

$$\begin{Bmatrix} t_n \\ t_t \\ t_b \end{Bmatrix} = \begin{bmatrix} \mathit{\Omega}_{nn} & 0 & 0 \\ 0 & \mathit{\Omega}_{tt} & 0 \\ 0 & 0 & \mathit{\Omega}_{bb} \end{bmatrix} \begin{Bmatrix} \mathit{\Delta}_n \\ \mathit{\Delta}_t \\ \mathit{\Delta}_b \end{Bmatrix} . \tag{3.4-1}$$

$$\mathbf{t} = \mathbf{\Omega} \quad \mathbf{\Delta} \tag{3.4-2}$$

The model distinguishes between a tension and compression loading for the stiffness component $\mathit{\Omega}_{nn}$:

$$\mathit{\Omega}_{nn} = \begin{cases} F_\mathrm{c}(\omega)\dfrac{\hat{t}_n}{\mathit{\Delta}_{n\mathrm{f}}} & \mathit{\Delta}_n \geq 0 \\ K_\mathrm{p} & \mathit{\Delta}_n < 0 \end{cases} , \tag{3.4-3}$$

where $F_\mathrm{c}(\omega)$ denotes a equation depending on damage evolution, ω the scalar damage variable, $\hat{t}_n$ the normal strength under tension loading, $\mathit{\Delta}_{n_\mathrm{f}}$ the displacement jump at rupture in normal direction and K_p a penalty stiffness. The behavior of this model in each single-mode is shown in Fig. 3.4-1(a). The stiffness in shear direction, Ω_{tt} and Ω_{bb}

$$\mathit{\Omega}_{tt} = F_\mathrm{c}(\omega)\frac{\hat{t}_\tau}{\mathit{\Delta}_{\tau\mathrm{f}}} \tag{3.4-4}$$

$$= \mathit{\Omega}_{bb} \tag{3.4-5}$$

depend on the strength in shear direction $\hat{t}_\tau$ and the displacement jump at rupture $\mathit{\Delta}_{\tau\mathrm{f}}$. The

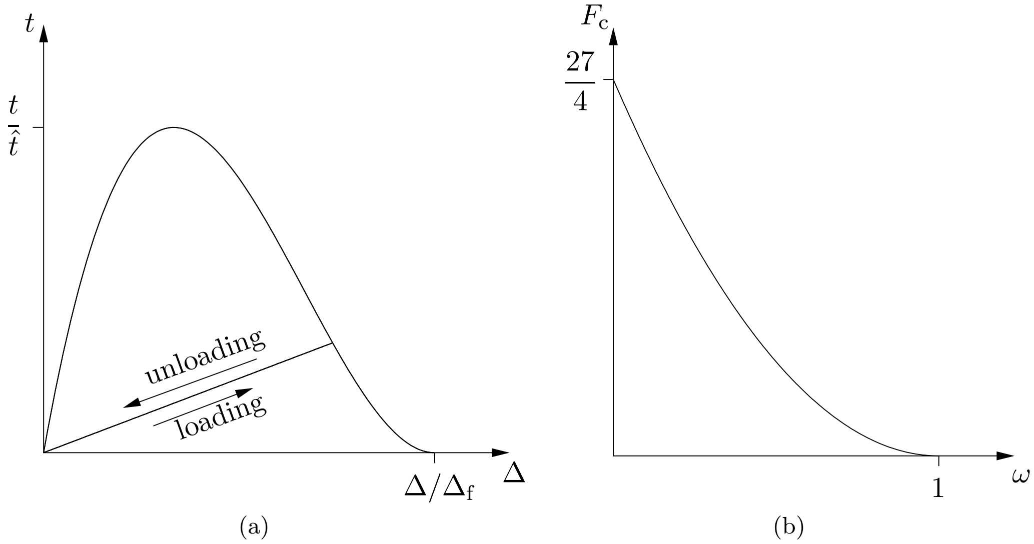

Fig. 3.4-1: Traction-separation-law by Chaboche in single-mode (a) Traction-separation relation (b) evolution of function F_c

damage evolution follows

$$F_\mathrm{c}(\omega) = \frac{27}{4}(1-\omega)^2 \tag{3.4-6}$$

and is shown in Fig. 3.4-1 (b). The damage variable ω is the maximum of the normed displacement jump in the loading history

$$\omega(t) = \mathcal{F}\left(\mathit{\Delta}_i(\tau)\right)_{\tau\geq-\infty}^{\tau=t} := \min\left\{\max_{\tau\leq t}|\mathit{\Delta}_i(\tau)|, 1\right\} \tag{3.4-7}$$

with the weighted norm

$$|\mathit{\Delta}_i(\tau)|_{\tau\leq t} = \sqrt{\left(\frac{\max\{0, \mathit{\Delta}_n(\tau)\}}{\mathit{\Delta}_{n\mathrm{f}}}\right)^2 + \left(\frac{\mathit{\Delta}_t(\tau)}{\mathit{\Delta}_{t\mathrm{f}}}\right)^2 + \left(\frac{\mathit{\Delta}_b(\tau)}{\mathit{\Delta}_{t\mathrm{f}}}\right)^2} \, . \tag{3.4-8}$$

The term $\max\{0, \mathit{\Delta}_n(\tau)\}$ guarantees only contributions due to a tensile loading

$$\max\{0, \mathit{\Delta}_n(\tau)\} = \begin{cases} \mathit{\Delta}_n & \mathit{\Delta}_n \geq 0 \\ 0 & \mathit{\Delta}_n \leq 0 \end{cases} \, . \tag{3.4-9}$$

3.4.2 Traction-Separation-Model by Lissenden

The traction-separation-law proposed by Lissenden [21], see Fig. 3.4-2 (a), has the same form such as Eq. (3.4-1) whereby the stiffness differ by the damage function $F_{\mathrm{L}}(\omega)$:

$$\mathit{\Omega}_{nn} = \begin{cases} F_{\mathrm{L}}(\omega)\dfrac{\hat{t}_n}{\mathit{\Delta}_{n\mathrm{f}}} & \mathit{\Delta}_n \geq 0 \\ K_{\mathrm{p}} & \mathit{\Delta}_n < 0 \end{cases} \tag{3.4-10}$$

$$\mathit{\Omega}_{tt} = F_{\mathrm{L}}(\omega)\frac{\hat{t}_\tau}{\mathit{\Delta}_{\tau\mathrm{f}}} \tag{3.4-11}$$

$$= \mathit{\Omega}_{bb} \, . \tag{3.4-12}$$

This damage function $F_{\mathrm{L}}(\omega)$, see Fig. 3.4-2 (b), is defined by

$$F_{\mathrm{L}}(\omega) = \frac{1 - 3\omega^2 + 2\omega^3}{\omega} \, . \tag{3.4-13}$$

The evolution of the scalar damage ω is given by Eq. (3.4-7) and the weighted norm $|\boldsymbol{\Delta}|$ by Eq. (3.4-8). The model does not have an initial stiffness. Softening occurs once the equivalent stress t_{v} is reached:

$$t_{\mathrm{v}}(t) := \min\left\{\max_{\tau\leq t}|\mathbf{t}(\tau)|, 1\right\} \, , \tag{3.4-14}$$

where the weighted traction norm $|\mathbf{t}(\tau)|$ is given by

$$||\mathbf{t}(\tau)||_{\tau\leq t} := \sqrt{\left(\frac{\max\{0, t_n(\tau)\}}{\hat{t}_n}\right)^2 + \left(\frac{t_t(\tau)}{\hat{t}_\tau}\right)^2 + \left(\frac{t_b(\tau)}{\hat{t}_\tau}\right)^2} \, . \tag{3.4-15}$$

3.4.3 Traction-Separation-Model by Camanho and Davila

Camanho and Davila [10] puplished a traction-separation-model based on the bilinear one of [15]. This elasto-damage model has an initial elastic stiffness K. The individual stiffness are given by

$$\mathit{\Omega}_{nn} = \left[1 - \mathrm{H}(\mathit{\Delta}_n)\omega\right]K \qquad \mathit{\Omega}_{tt} = (1-\omega)K \qquad \mathit{\Omega}_{bb} = (1-\omega)K \tag{3.4-16}$$

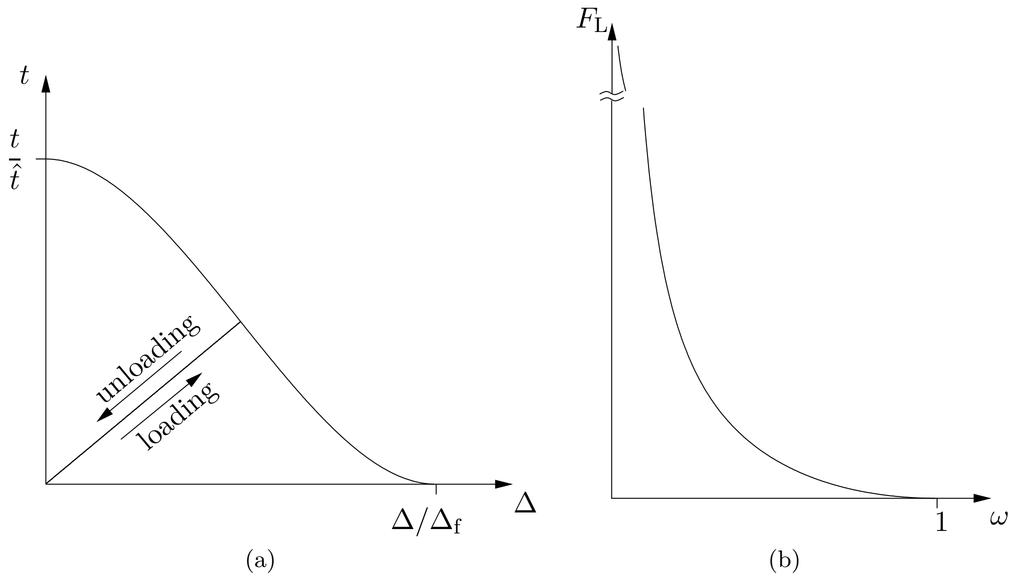

Fig. 3.4-2: Traction-separation-law by Lissenden in single-mode (a) Traction-separation relation (b) evolution of function F_L

where the HEAVISIDE-function $\mathrm{H}(\mathit{\Delta}_n)$ is defined by

$$\mathrm{H}(\mathit{\Delta}_n) = \begin{cases} 1 & \mathit{\Delta}_n \geq 0 \\ 0 & \mathit{\Delta}_n < 0 \end{cases} . \tag{3.4-17}$$

Damage starts once the quadratic stress criterion

$$f(t_n, t_\tau) = \sqrt{\left(\frac{\langle t_n \rangle}{\hat{t}_n}\right)^2 + \left(\frac{t_\tau}{\hat{t}_\tau}\right)^2} - 1 = 0 \tag{3.4-18}$$

proposed by [8] is reached. The algebraic equation for damage evolution follows

$$\omega(q_\mathrm{m}, \mathit{\Delta}_\mathrm{m}^\mathrm{max}, \mathit{\Delta}_\mathrm{mc}) = \frac{q_\mathrm{m}(\mathit{\Delta}_\mathrm{m}^\mathrm{max} - \mathit{\Delta}_\mathrm{mc})}{(q_\mathrm{m} - 1)\mathit{\Delta}_\mathrm{m}^\mathrm{max}} . \tag{3.4-19}$$

A mixed-mode path Δ_m describes mixed-mode loading:

$$\mathit{\Delta}_\mathrm{m}(\mathit{\Delta}_n, \mathit{\Delta}_\tau) = \sqrt{\langle \mathit{\Delta}_n \rangle^2 + \mathit{\Delta}_\tau^2} \tag{3.4-20}$$

where $\langle . \rangle$ denotes the MACAULEY-brackets:

$$\langle x \rangle = \begin{cases} x & x \geq 0 \\ 0 & x < 0 \end{cases} . \tag{3.4-21}$$

A mixity ratio β is introduced for the range $\Delta_n > 0$:

$$\beta(\mathit{\Delta}_\tau, \mathit{\Delta}_n) = \frac{\mathit{\Delta}_\tau}{\mathit{\Delta}_n} \qquad \mathit{\Delta}_n > 0 . \tag{3.4-22}$$

A critical mixed-mode displacement jump Δ_{mc} is the displacement-based formulation of the stress criterion (3.4-18), see [15]:

$$\varDelta_{\mathrm{mc}}(\beta) = \varDelta_{\tau\mathrm{c}}\sqrt{\frac{1+\beta^2}{\beta_{\mathrm{c}}^2+\beta^2}} \quad \forall\ \varDelta_n > 0\,,\ \beta > 0 \quad \text{with} \quad \beta_{\mathrm{c}} := \frac{\varDelta_{\tau\mathrm{c}}}{\varDelta_{n\mathrm{c}}}\ . \tag{3.4-23}$$

The power-law fracture criterion of Whitcomb [27]

$$f^*(\Gamma_n^*, \Gamma_\tau^*) = \left(\frac{\Gamma_n^*\,\mathrm{H}(\varDelta_n)}{\Gamma_{n\mathrm{c}}}\right)^{\eta} + \left(\frac{\Gamma_\tau^*}{\Gamma_{\tau\mathrm{c}}}\right)^{\eta} - 1 = 0 \tag{3.4-24}$$

defined with strain energy release rates Γ_n^*, Γ_τ^* of mode-I and mode-II as well as the interaction parameter η is reformulated to use it in its displacement-based form characterized by the scalar factor q_{m}, see [9]:

$$q_{\mathrm{m}}(\beta) = (\beta_{\mathrm{c}}^2+\beta^2)\left[\left(\frac{\beta_{\mathrm{c}}^2}{q_n}\right)^{\bar{\eta}} + \left(\frac{\beta^2}{q_\tau}\right)^{\bar{\eta}}\right]^{-\frac{1}{\bar{\eta}}} \qquad \beta > 0\ . \tag{3.4-25}$$

3.5 Assembling to RUC System of Equations

The assembling process of setting the condensed microstructure system of equations up is conducted by applying the direct stiffness method. Therefore, global degrees of freedom $\bar{\mathbf{r}}'$ are introduced. In the case of perfect bounding, see Eqs. (3.5-1) through (3.5-2), the assembling leads from six local to three global degrees of freedom between adjacent subcells since they are the same in this case:

$$\bar{\mathbf{u}}'^{2-(\beta,\gamma)} = \bar{\mathbf{u}}'^{2+(\beta-1,\gamma)} \tag{3.5-1}$$

$$\bar{\mathbf{u}}'^{3-(\beta,\gamma)} = \bar{\mathbf{u}}'^{3+(\beta,\gamma-1)}\ . \tag{3.5-2}$$

Using of interface subcells between adjacent solid-subcells increase the number of global degrees of freedom by three additional ones. The defining of global degrees of freedom is illustrated in Fig. 3.5-1 for both cases. The number of unknowns amount to $N_{\mathrm{DOF}} = 6N_\beta N_\gamma$ in the case of perfect bonding and $N_{\mathrm{DOF}} = 6N_\beta N_\gamma + 3N_{\mathrm{Int}}$ in the event of imperfect bonding (using N_{Int} interface-subcells). The conditions of traction continuity generate the equations in the case of perfect bonding, in particular the traction continuity between adjacent solid-subcells in the sectoral plane (z_1, z_3) with the unit vector $\mathbf{n} = \mathbf{e}_2$:

$$\bar{\mathbf{t}}^{2+(\beta,\gamma)} + \bar{\mathbf{t}}^{2-(\beta+1,\gamma)} = \mathbf{0} \qquad \beta = 1,...,N_\beta - 1\ ;\ \gamma = 1,...,N_\gamma\ , \tag{3.5-3}$$

and in the sectoral plane (z_1, z_2) with the unit vector $\mathbf{n} = \mathbf{e}_3$:

$$\bar{\mathbf{t}}^{3+(\beta,\gamma)} + \bar{\mathbf{t}}^{3-(\beta,\gamma+1)} = \mathbf{0} \qquad \beta = 1,...,N_\beta\ ;\ \gamma = 1,...,N_\gamma - 1 \tag{3.5-4}$$

as well as the periodic traction conditions:

$$\bar{\mathbf{t}}^{2-(1,\gamma)} + \bar{\mathbf{t}}^{2+(N_\beta,\gamma)} = \mathbf{0} \qquad \text{for} \quad \mathbf{n} = \mathbf{e}_2 \tag{3.5-5}$$

$$\bar{\mathbf{t}}^{3-(\beta,1)} + \bar{\mathbf{t}}^{3+(\beta,N_\gamma)} = \mathbf{0} \qquad \text{for} \quad \mathbf{n} = \mathbf{e}_3\ . \tag{3.5-6}$$

In the case of imperfect bonding the interface system of equations (3.3-9) provides the basic equations, which yield for an interface-subcell inserted between the subcells $\Omega^{(\beta,\gamma)}$ and $\Omega^{(\beta+1,\gamma)}$

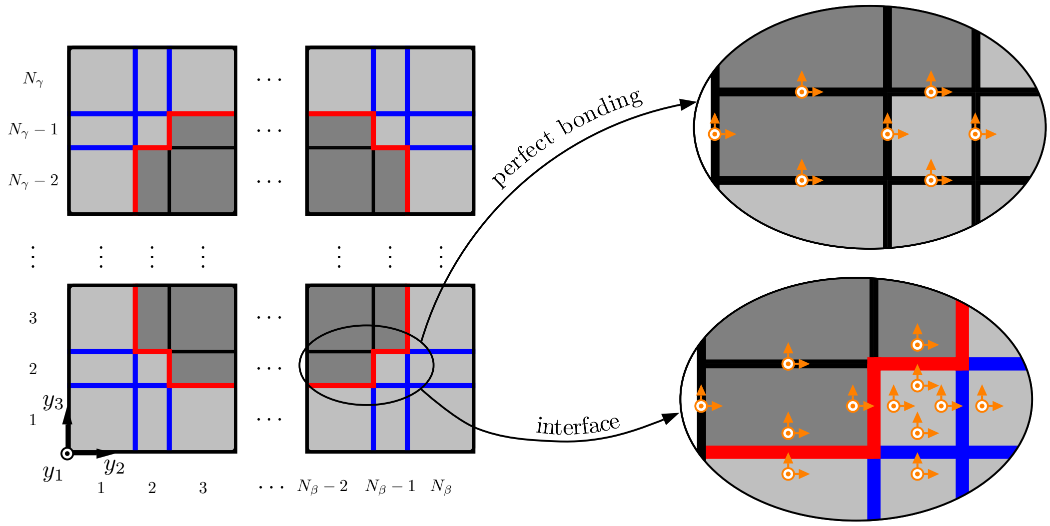

Fig. 3.5-1: Global degrees of freedom in case of perfect bonding between solid-subcells and interface-subcells between adjacent solid-subcells

$(\mathbf{n} = \mathbf{e}_2)$:

$$\begin{aligned} \bar{\mathbf{t}}^{2+(\beta,\gamma)} &= \mathbf{I}^{2(j)}\bar{\mathbf{u}}'^{2+(\beta,\gamma)} && \beta = 1,\ldots,N_\beta - 1; \quad \gamma = 1,\ldots,N_\gamma \\ \bar{\mathbf{t}}^{2-(\beta+1,\gamma)} &= \mathbf{I}^{2(j)}\bar{\mathbf{u}}'^{2-(\beta+1,\gamma)} && \beta = 1,\ldots,N_\beta - 1; \quad \gamma = 1,\ldots,N_\gamma \end{aligned} \tag{3.5-7}$$

and for an interface-subcell between the subcells $\Omega^{(\beta,\gamma)}$ and $\Omega^{(\beta,\gamma+1)}$ $(\mathbf{n} = \mathbf{e}_3)$:

$$\begin{aligned} \bar{\mathbf{t}}^{3+(\beta,\gamma)} &= \mathbf{I}^{3(j)}\bar{\mathbf{u}}'^{3+(\beta,\gamma)} && \beta = 1,...,N_\beta; \quad \gamma = 1,...,N_\gamma - 1 \\ \bar{\mathbf{t}}^{3-(\beta,\gamma+1)} &= \mathbf{I}^{3(j)}\bar{\mathbf{u}}'^{3-(\beta,\gamma+1)} && \beta = 1,...,N_\beta; \quad \gamma = 1,...,N_\gamma - 1 \quad . \end{aligned} \tag{3.5-8}$$

Assessing the conditions of tractions continuity shown previously, the overall RUC system of equations is obtained:

$$\left[\widehat{\mathbf{K}} - \widehat{\mathbf{I}}(\bar{\mathbf{r}}')\right]\bar{\mathbf{r}}' = -\widehat{\mathbf{D}}\boldsymbol{\varepsilon}^0 \ . \tag{3.5-9}$$

The global stiffness matrix $\widehat{\mathbf{K}}$ of all solid-subcells and the global matrix $\widehat{\mathbf{I}}$ of all inserted interface-subcells have the dimension $\widehat{\mathbf{K}} \in \mathbb{R}^{N_{\text{DOF}} \times N_{\text{DOF}}}$ and $\widehat{\mathbf{I}} \in \mathbb{R}^{N_{\text{DOF}} \times N_{\text{DOF}}}$. The stiffness matrix $\widehat{\mathbf{K}}$ is not symmetric

$$\widehat{\mathbf{K}} \neq \widehat{\mathbf{K}}^{\mathrm{T}} \quad \forall\ l_2^{(\beta)} \neq l_3^{(\gamma)} \tag{3.5-10}$$

for rectangular subcells, but for quadratic ones:

$$\widehat{\mathbf{K}} = \widehat{\mathbf{K}}^{\mathrm{T}} \quad \forall\ l_2^{(\beta)} = l_3^{(\gamma)} \ . \tag{3.5-11}$$

The stiffness matrix of all interface-subcells is always symmetric

$$\widehat{\mathbf{I}} = \widehat{\mathbf{I}}^{\mathrm{T}} \qquad \forall\ l_2^{(\beta)} \neq l_3^{(\gamma)},\ l_2^{(\beta)} = l_3^{(\beta)} \ . \tag{3.5-12}$$

To assemble the matrices $\widehat{\mathbf{K}}$, $\widehat{\mathbf{I}}$ and $\widehat{\mathbf{D}}$ by applying the direct stiffness method, location-matrices are introduced for each solid-subcell:

$$\mathbf{m}^{(\beta,\gamma)} = \{m_1 \ \ m_2 \ \ m_3 \ \ m_4 \ \ m_5 \ \ m_6 \ \ m_7 \ \ m_8 \ \ m_9 \ \ m_{10} \ \ m_{11} \ \ m_{12}\}^{(\beta,\gamma)^{\mathsf{T}}} \tag{3.5-13}$$

and for each interface-subcell

$$\widetilde{\mathbf{m}}^{n(j)} = \{\tilde{m}_1 \quad \tilde{m}_2 \quad \tilde{m}_3 \quad \tilde{m}_4 \quad \tilde{m}_5 \quad \tilde{m}_6\}^{n(j)^\mathsf{T}} . \tag{3.5-14}$$

The location-matrices (3.5-13) and (3.5-14) are visualized in Fig. 3.5-2 (a) and 3.5-2 (b). The order of the components is based on the order of the degrees of freedom in the solid-subcell system of equations (3.2-33) and interface-subcell system of equations (3.3-9). These matrices are filled by the number of the global degrees of freedom $\bar{\mathbf{r}}'$ allocated previously. The interface-subcells share their global degrees of freedom with adjacent solid-subcells and depend on its orientation. Hence, the entries of the interface location-matrix are certain entries of the location matrix of solid-subcells:

$$\widetilde{\mathbf{m}}^{2(j)} = \left\{m_4^{(\beta,\gamma)}, m_6^{(\beta,\gamma)}, m_2^{(\beta,\gamma)}, m_3^{(\beta-1,\gamma)}, m_5^{(\beta-1,\gamma)}, m_1^{(\beta-1,\gamma)}\right\}^{2(j)^\mathsf{T}} \tag{3.5-15}$$

$$\widetilde{\mathbf{m}}^{3(j)} = \left\{m_{12}^{(\beta,\gamma)}, m_{10}^{(\beta,\gamma)}, m_8^{(\beta,\gamma)}, m_{11}^{(\beta,\gamma-1)}, m_9^{(\beta,\gamma-1)}, m_7^{(\beta,\gamma-1)}\right\}^{3(j)^\mathsf{T}} . \tag{3.5-16}$$

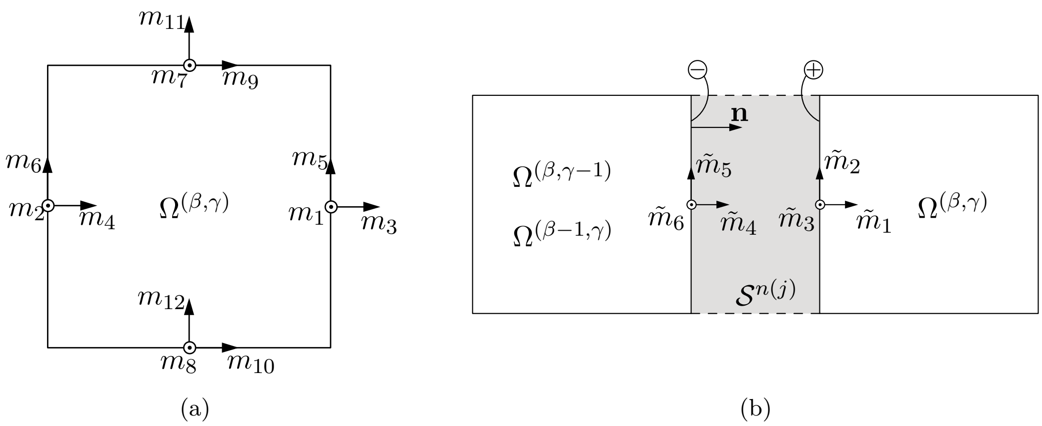

Fig. 3.5-2: (a) Components of location matrix of solid-subcell $\Omega^{(\beta,\gamma)}$ (b) Components of location matrix of interface-subcell $\mathcal{S}^{n(j)}$ between subcell $\Omega^{(\beta,\gamma-1)}$ and $\Omega^{(\beta,\gamma)}$ or $\Omega^{(\beta-1,\gamma)}$ and $\Omega^{(\beta,\gamma)}$

Ultimately, the assembling of the global matrices $\widehat{\mathbf{K}}, \widehat{\mathbf{I}}$ and $\widehat{\mathbf{D}}$ is a summation process:

$$\begin{aligned}
\widehat{K}_{lk} &= \sum_{\beta=1}^{N_\beta}\sum_{\gamma=1}^{N_\gamma}\sum_{i=1}^{12}\sum_{j=1}^{12} K_{ij}^{(\beta,\gamma)} \quad &&\text{with} \quad l = m_i^{(\beta,\gamma)}, \, k = m_j^{(\beta,\gamma)} \\
\widehat{D}_{lk} &= \sum_{\beta=1}^{N_\beta}\sum_{\gamma=1}^{N_\gamma}\sum_{i=1}^{12}\sum_{j=1}^{6} D_{ij}^{(\beta,\gamma)} \quad &&\text{with} \quad l = m_i^{(\beta,\gamma)}, \, k = m_j^{(\beta,\gamma)} \\
\widehat{I}_{lk} &= \sum_{n=1}^{N_{\text{Int}}}\sum_{i=1}^{6}\sum_{j=1}^{6} I_{ij}^{n(j)} \quad &&\text{with} \quad l = m_i^{n(j)}, \, k = m_j^{n(j)} \, .
\end{aligned} \tag{3.5-17}$$

These summations can be “visualized” by writing the location-matrices $\mathbf{m}^{(\beta,\gamma)}$ and $\widetilde{\mathbf{m}}^{n(j)}$ along the columns and rows of the solid-subcell stiffness $\mathbf{K}^{(\beta,\gamma)}$, matrix comprising material stiffness $\mathbf{D}^{(\beta,\gamma)}$ and interface-subcell stiffness matrix $\mathbf{I}^{n(j)}$ as follows

$$\{\, m_1 \quad m_2 \quad \dots \quad m_{11} \quad m_{12} \,\}$$

$$\begin{Bmatrix} m_1 \\ m_2 \\ \vdots \\ m_{11} \\ m_{12} \end{Bmatrix} \begin{bmatrix} K_{1,1} & K_{1,2} & \dots & 0 & 0 \\ K_{2,1} & K_{2,2} & \dots & 0 & 0 \\ \vdots & \vdots & \ddots & \vdots & \vdots \\ 0 & 0 & \dots & K_{11,11} & K_{11,12} \\ 0 & 0 & \dots & K_{12,11} & K_{12,12} \end{bmatrix} \tag{3.5-18}$$

$$\begin{array}{cc} & \{\begin{matrix} 1 & 2 & 3 & 4 & 5 & 6 \end{matrix}\} \\ \begin{Bmatrix} m_1 \\ m_2 \\ \vdots \\ m_{11} \\ m_{12} \end{Bmatrix} & \begin{bmatrix} 0 & 0 & 0 & 0 & D_{15} & 0 \\ 0 & 0 & 0 & 0 & D_{25} & 0 \\ \vdots & \vdots & \vdots & \vdots & \vdots & \vdots \\ D_{51} & D_{52} & D_{53} & 0 & 0 & 0 \\ D_{61} & D_{62} & D_{63} & 0 & 0 & 0 \end{bmatrix} \end{array} \tag{3.5-19}$$

$$\begin{array}{cc} & \{\begin{matrix} \widetilde{m}_1 & \widetilde{m}_2 & \widetilde{m}_3 & \widetilde{m}_4 & \widetilde{m}_5 & \widetilde{m}_6 \end{matrix}\} \\ \begin{Bmatrix} \widetilde{m}_1 \\ \widetilde{m}_2 \\ \widetilde{m}_3 \\ \widetilde{m}_4 \\ \widetilde{m}_5 \\ \widetilde{m}_6 \end{Bmatrix} & \begin{bmatrix} I_{11} & 0 & 0 & I_{14} & 0 & 0 \\ 0 & I_{22} & 0 & 0 & I_{25} & 0 \\ 0 & 0 & I_{33} & 0 & 0 & I_{36} \\ I_{41} & 0 & 0 & I_{44} & 0 & 0 \\ 0 & I_{52} & 0 & 0 & I_{55} & 0 \\ 0 & 0 & I_{63} & 0 & 0 & I_{66} \end{bmatrix} \end{array} . \tag{3.5-20}$$

The resultant system of equations comprises rigid body motions, i. e. the stiffness matrix is

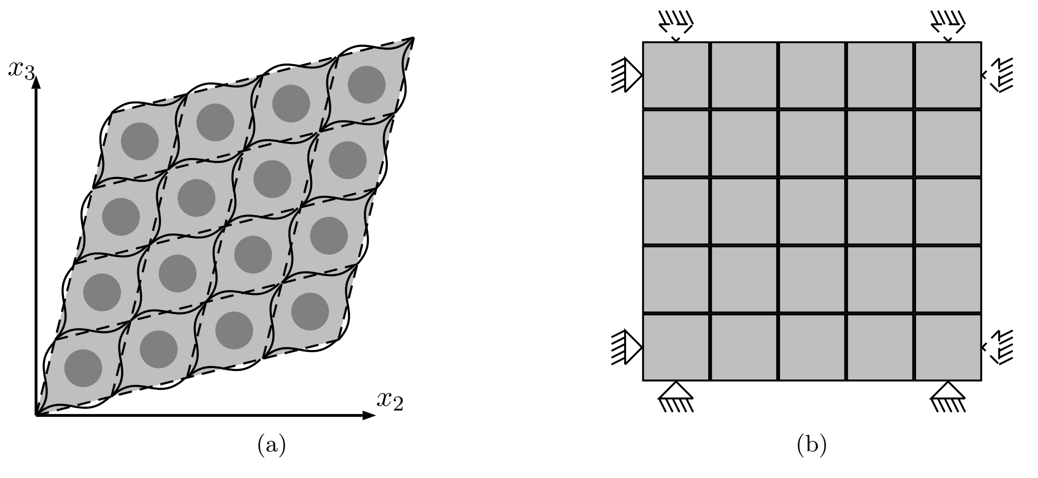

Fig. 3.5-3: (a) Homogeneous and periodic deformation of RVE with periodic micro structure and each RUC under macro shear strain $\varepsilon^0_{23} = \varepsilon^0_{32}$ [19] (b) Bearing of discretized RUC [19]

singular. Every surface-averaged displacement of one corner cell (bottom left) is restraint and the surface-averaged displacement of two more corner cells at the respective edges (bottom right and top left), see Fig. 3.5-3 (b) marked with solid symbols. Three degrees of freedom are restraint at four faces. So, the number of unknowns N_{DOF} becomes

$$N_{\text{DOF}} = 6N_\beta N_\gamma + 3N_{\text{Int}} - 12 \; . \tag{3.5-21}$$

Because of the periodic boundary conditions, the degrees of freedom of opposite solid-subcell surfaces are restraint as well, see Fig. 3.5-3 (b) marked with dashed symbols. The bearing is taken into account by a zero in the appropriate entry of the solid-subcell location-matrix.

3.6 Effective Stiffness

The effective macro stiffness $\mathbf{C}^*$ is the derivation of the macro stress $\boldsymbol{\sigma}^0 = \langle\boldsymbol{\sigma}\rangle$ with respect to the macro strain $\boldsymbol{\varepsilon}^0$

$$\mathbf{C}^* = \frac{\partial\boldsymbol{\sigma}^0}{\partial\boldsymbol{\varepsilon}^0} = \frac{\partial\langle\boldsymbol{\sigma}\rangle}{\partial\boldsymbol{\varepsilon}^0} \ . \tag{3.6-1}$$

The subcell-averaged strain in each subcell $\langle\boldsymbol{\varepsilon}^{(\beta,\gamma)}\rangle$ consists of a macro part being constant and a fluctuating contribution, see Eqs. (3.1-13) through (3.1-18). The microvariables $\mathbf{W}_{(nm)}$ in the fluctuating part are replaced by the unknown averaged surface displacements $\bar{\mathbf{u}}'^{(\beta,\gamma)}$ by using Eqs. (3.2-20) through (3.2-25) and a relation for the fluctuating part of the subcell-averaged strain:

$$\tilde{\boldsymbol{\varepsilon}}^{(\beta,\gamma)} = \mathbf{Y}^{(\beta,\gamma)}\,\bar{\mathbf{u}}'^{(\beta,\gamma)} \tag{3.6-2}$$

with

$$\mathbf{Y}^{(\beta,\gamma)} = \begin{bmatrix} 0 & 0 & 0 & 0 & 0 & 0 & 0 & 0 & 0 & 0 & 0 & 0 \\ 0 & 0 & Y_{23} & Y_{24} & 0 & 0 & 0 & 0 & 0 & 0 & 0 & 0 \\ 0 & 0 & 0 & 0 & 0 & 0 & 0 & 0 & 0 & 0 & Y_{3,11} & Y_{3,12} \\ 0 & 0 & 0 & 0 & Y_{45} & Y_{46} & 0 & 0 & Y_{49} & Y_{4,10} & 0 & 0 \\ Y_{51} & Y_{52} & 0 & 0 & 0 & 0 & 0 & 0 & 0 & 0 & 0 & 0 \\ 0 & 0 & 0 & 0 & 0 & 0 & Y_{67} & Y_{68} & 0 & 0 & 0 & 0 \end{bmatrix}^{(\beta,\gamma)} . \tag{3.6-3}$$

The non-zero entries of the matrix $\mathbf{Y}$ are given by

$$\mathrm{Y}_{23} = -\mathrm{Y}_{24} = 2\mathrm{Y}_{45} = -2\mathrm{Y}_{46} = 2\mathrm{Y}_{51} = -2\mathrm{Y}_{52} = \frac{1}{l_2^{(\beta)}} \tag{3.6-4}$$

$$\mathrm{Y}_{3,11} = -\mathrm{Y}_{3,12} = 2\mathrm{Y}_{49} = -2\mathrm{Y}_{4,10} = 2\mathrm{Y}_{67} = -2\mathrm{Y}_{68} = \frac{1}{l_3^{(\gamma)}} \ . \tag{3.6-5}$$

The subcell-averaged strain, see Eqs. (3.1-13) through (3.1-18), becomes with Eq. (3.6-2):

$$\langle\boldsymbol{\varepsilon}^{(\beta,\gamma)}\rangle = \boldsymbol{\varepsilon}^0 + \mathbf{Y}^{(\beta,\gamma)}\,\bar{\mathbf{u}}'^{(\beta,\gamma)} \ . \tag{3.6-6}$$

Using Eq. (3.1-20) and Eq. (3.6-6), the constitutive relation of each subcell may be written as

$$\langle\boldsymbol{\sigma}^{(\beta,\gamma)}\rangle = \mathbf{C}^{(\beta,\gamma)}\left(\boldsymbol{\varepsilon}^0 + \mathbf{Y}^{(\beta,\gamma)}\,\bar{\mathbf{u}}'^{(\beta,\gamma)}\right) \ . \tag{3.6-7}$$

The sum of Eq. (3.1-22) is rewritten with Eq. (3.6-7):

$$\langle\boldsymbol{\sigma}\rangle = \frac{1}{L_2\,L_3}\left(\sum_{\beta=1}^{N_\beta}\sum_{\gamma=1}^{N_\gamma} l_2^{(\beta)} l_3^{(\gamma)}\mathbf{C}^{(\beta,\gamma)}\boldsymbol{\varepsilon}^0 + \sum_{\beta=1}^{N_\beta}\sum_{\gamma=1}^{N_\gamma} l_2^{(\beta)} l_3^{(\gamma)}\mathbf{C}^{(\beta,\gamma)}\mathbf{Y}^{(\beta,\gamma)}\,\bar{\mathbf{u}}'^{(\beta,\gamma)}\right) \tag{3.6-8}$$

Hence, the effective stiffness (3.6-1) is obtained[1] by using Eq. (3.6-8)

$$C^*_{ki} = \frac{1}{L_2\,L_3}\left(\sum_{\beta=1}^{N_\beta}\sum_{\gamma=1}^{N_\gamma} l_2^{(\beta)} l_3^{(\gamma)} \mathrm{C}_{ki}^{(\beta\gamma)} + \sum_{\beta=1}^{N_\beta}\sum_{\gamma=1}^{N_\gamma} l_2^{(\beta)} l_3^{(\gamma)} \mathrm{C}_{kl}^{(\beta\gamma)} \mathrm{Y}_{lj}^{(\beta\gamma)} \frac{\partial \bar{\mathrm{u}}_j^{\prime(\beta\gamma)}}{\partial \varepsilon^*_i}\right) . \tag{3.6-9}$$

The unknown derivation $\partial \bar{u}_j^{\prime(\beta\gamma)}/\partial\varepsilon_i^0$ is calculated by differentiating the RUC system of equation (3.5-9) with respect to the macro strain ε_i^0

$$\frac{\partial}{\partial \varepsilon_l^0}\left\{\left[\widehat{K}_{ij} - \widehat{I}_{ij}(\widehat{\bar{r}}'_j)\right]\widehat{\bar{r}}'_j\right\} = \frac{\partial}{\partial \varepsilon_l}\left\{-\widehat{D}_{ij}\varepsilon_j^0\right\} . \tag{3.6-10}$$

Applying the product and chain rule, Eq. (3.6-10) becomes:

$$\frac{\partial\left[\widehat{K}_{ij} - \widehat{I}_{ij}(\widehat{\bar{r}}'_j)\right]}{\partial \widehat{\bar{r}}'_m}\frac{\partial \widehat{\bar{r}}'_m}{\partial \varepsilon_l^0}\widehat{\bar{r}}'_j + \left[\widehat{K}_{ij} - \widehat{I}_{ij}(\widehat{\bar{r}}'_j)\right]\frac{\partial \widehat{\bar{r}}'_j}{\partial \varepsilon_l^0} = -\widehat{D}_{ij}\delta_{jl} . \tag{3.6-11}$$

Substituting the silent index of the second summand and bracketing leads to

$$\left\{\frac{\partial\left[\widehat{K}_{ij} - \widehat{I}_{ij}(\widehat{\bar{r}}'_j)\right]}{\partial \widehat{\bar{r}}'_m}\widehat{\bar{r}}'_j + \left[\widehat{K}_{im} - \widehat{I}_{im}(\widehat{\bar{r}}'_m)\right]\right\}\frac{\partial \widehat{\bar{r}}'_m}{\partial \varepsilon_l^0} = -\widehat{D}_{il} \tag{3.6-12}$$

$$\underbrace{\left\{\frac{\partial\left[-\widehat{I}_{ij}(\widehat{\bar{r}}'_j)\right]}{\partial \widehat{\bar{r}}'_m}\widehat{\bar{r}}'_j + \left[\widehat{K}_{im} - \widehat{I}_{im}(\widehat{\bar{r}}'_m)\right]\right\}}_{\widehat{K}_{il}^{\mathrm{Tan}}}\frac{\partial \widehat{\bar{r}}'_m}{\partial \varepsilon_l^0} = -\widehat{I}_{il} . \tag{3.6-13}$$

The term in the brackets of Eq. (3.6-13) is the tangent stiffness matrix $\widehat{\mathbf{K}}^{\mathrm{Tan}}$ resulting from the linearization of the nonlinear system of equations (3.5-9), which is shown in the next section. So a linear system of equations must be solved for six different right-hand-sides to get the derivative $\partial\bar{\mathbf{r}}'/\partial\boldsymbol{\varepsilon}^0$. The entries needed for the derivative $\partial\bar{\mathbf{u}}'^{(\beta,\gamma)}/\partial\boldsymbol{\varepsilon}^0$ is picked out by the use of the location-matrix $\mathbf{m}^{(\beta,\gamma)}$ of the solid-subcell considered.

3.7 Consistent Linearization of Micromechanical System of Equations

Newton's method for finding the root of a real-valued function is based on a first order approximation of this function at a real point. For that, the nonlinear system of equations (3.5-9) is transformed into a residual equation

$$\mathbf{r}(\bar{\mathbf{r}}') = \left[\widehat{\mathbf{K}} - \widehat{\mathbf{I}}(\bar{\mathbf{r}}')\right]\bar{\mathbf{r}}' + \widehat{\mathbf{D}}\boldsymbol{\varepsilon}^0 . \tag{3.7-1}$$

The iteration rule of Newton's method

$$\mathbf{r}(\bar{\mathbf{r}}'^{\,i+1}_{n+1}) = \mathbf{r}(\bar{\mathbf{r}}'^{\,i}_{n+1}) + \mathrm{D}\mathbf{r}(\Delta\bar{\mathbf{r}}'^{\,i+1}_{n+1}) \tag{3.7-2}$$

[1] Index notation is used to show matrix multiplication

needs the Gâuteaux-differential of Eq. (3.7-1)

$$
\begin{aligned}
\mathrm{D}\mathbf{r}[\Delta\bar{\mathbf{r}}'] &= \frac{\mathrm{d}}{\mathrm{d}\eta}\left[\mathbf{r}\left(\bar{\mathbf{r}}' + \eta\Delta\bar{\mathbf{r}}'\right)\right]_{\eta=0} && (3.7\text{-}3)\\
&= \left[\widehat{\mathbf{K}} - \widehat{\mathbf{I}}\left(\bar{\mathbf{r}}'\right)\right]\,\Delta\bar{\mathbf{r}}' + \frac{\partial\left[\widehat{\mathbf{K}} - \widehat{\mathbf{I}}\left(\bar{\mathbf{r}}'\right)\right]}{\partial\bar{\mathbf{r}}'}\,\Delta\bar{\mathbf{r}}'\,\bar{\mathbf{r}}' && (3.7\text{-}4)\\
&= \left[\widehat{\mathbf{K}} - \widehat{\mathbf{I}}\left(\bar{\mathbf{r}}'\right)\right]\,\Delta\bar{\mathbf{r}}' - \frac{\partial\,\widehat{\mathbf{L}}\left(\bar{\mathbf{r}}'\right)}{\partial\,\bar{\mathbf{r}}'}\,\Delta\bar{\mathbf{r}}'\,\bar{\mathbf{r}}'\ . && (3.7\text{-}5)
\end{aligned}
$$

The calculation rule becomes visible in index notation:

$$
\begin{aligned}
\mathrm{D}r_i[\Delta\bar{r}'_j] &= \left[\widehat{K}_{ij} - \widehat{I}_{ij}\left(\bar{r}'_j\right)\right]\Delta\bar{r}'_k - \widehat{I}_{ik,j}\,\Delta\bar{r}'_j\,\bar{r}'_k && (3.7\text{-}6)\\
&= \underbrace{\left\{\left[\widehat{K}_{ij} - \widehat{I}_{ij}\left(\bar{r}'_j\right)\right] - \widehat{I}_{ik,j}\,\bar{r}'_k\right\}}_{=\,\widehat{K}^{\mathrm{Tan}}_{ij}}\,\Delta\bar{r}'_j\ , && (3.7\text{-}7)
\end{aligned}
$$

which reveals the linearized stiffness matrix $\widehat{\mathbf{K}}^{\mathrm{Tan}}$. The linear system of equations

$$
\widehat{\mathbf{K}}^{\mathrm{Tan}}\left(\bar{\mathbf{r}}'^{\,i}_{(n+1)}\right)\Delta\bar{\mathbf{r}}'^{\,i+1}_{(n+1)} = -\mathbf{r}\left(\bar{\mathbf{r}}'^{\,i}_{(n+1)}\right) \qquad (3.7\text{-}8)
$$

is solved in each iteration step i to update the approximation for the root $\bar{\mathbf{r}}'^{\,i+1}_{(n+1)}$:

$$
\bar{\mathbf{r}}'^{\,i+1}_{(n+1)} = \bar{\mathbf{r}}'^{\,i}_{(n+1)} + \Delta\bar{\mathbf{r}}'^{\,i+1}_{(n+1)}\ . \qquad (3.7\text{-}9)
$$

The matrix $\widehat{I}'_{ij} = \widehat{I}_{ik,j}\bar{r}'_k$ is build up in each iteration step next to the matrices $\widehat{K}_{ij}$ and $\widehat{I}_{ij}$ to form $\widehat{K}^{\mathrm{Tan}}_{ij}$ by applying the direct stiffness method. First, the linearized stiffness matrix $K^{\mathrm{Tan}}_{ij} = I_{ik,j}\bar{u}'^{i\pm}_k$ is calculated at the local level and afterwards assembled, which is formally a summation process:

$$
\widehat{I}'_{lk} = \sum_{n=1}^{N_{\mathrm{Int}}}\sum_{i=1}^{6}\sum_{j=1}^{6} I^{(n)'}_{ij} \quad \text{with} \quad l = \tilde{m}^{(n)}_i\ ,\ k = \tilde{m}^{(n)}_j\ . \qquad (3.7\text{-}10)
$$

Once again, this process can be “visualized” by writing the location-matrix of each interface-subcell along the rows and columns:

$$
\begin{array}{cc}
 & \{\,\tilde{m}_1 \quad \tilde{m}_2 \quad \tilde{m}_3 \quad \tilde{m}_4 \quad \tilde{m}_5 \quad \tilde{m}_6\,\} \\
\begin{Bmatrix} \tilde{m}_1 \\ \tilde{m}_2 \\ \tilde{m}_3 \\ \tilde{m}_4 \\ \tilde{m}_5 \\ \tilde{m}_6 \end{Bmatrix} &
\begin{bmatrix}
I'_{11} & I'_{12} & I'_{13} & I'_{14} & I'_{15} & I'_{16}\\
I'_{21} & I'_{22} & I'_{23} & I'_{24} & I'_{25} & I'_{26}\\
I'_{31} & I'_{32} & I'_{33} & I'_{34} & I'_{35} & I'_{36}\\
I'_{41} & I'_{42} & I'_{43} & I'_{44} & I'_{45} & I'_{46}\\
I'_{51} & I'_{52} & I'_{53} & I'_{54} & I'_{55} & I'_{56}\\
I'_{61} & I'_{62} & I'_{63} & I'_{64} & I'_{65} & I'_{66}
\end{bmatrix}^{n(j)}
\end{array}
\ . \qquad (3.7\text{-}11)
$$

The several entries of the matrix $\widehat{I}_{ij}^{n(j)'}$ are:

$$\hat{I}_{ij}^{n(j)'} = \begin{bmatrix} -\frac{\partial \Omega_{nn}}{\partial \bar{u}_n^+}\Delta_n & -\frac{\partial \Omega_{nn}}{\partial \bar{u}_t^+}\Delta_n & -\frac{\partial \Omega_{nn}}{\partial \bar{u}_b^+}\Delta_n & \frac{\partial \Omega_{nn}}{\partial \bar{u}_n^-}\Delta_n & \frac{\partial \Omega_{nn}}{\partial \bar{u}_t^-}\Delta_n & \frac{\partial \Omega_{nn}}{\partial \bar{u}_b^-}\Delta_n \\ -\frac{\partial \Omega_{tt}}{\partial \bar{u}_n^+}\Delta_t & -\frac{\partial \Omega_{tt}}{\partial \bar{u}_t^+}\Delta_t & -\frac{\partial \Omega_{tt}}{\partial \bar{u}_b^+}\Delta_t & \frac{\partial \Omega_{tt}}{\partial \bar{u}_n^-}\Delta_t & \frac{\partial \Omega_{tt}}{\partial \bar{u}_t^-}\Delta_t & \frac{\partial \Omega_{tt}}{\partial \bar{u}_b^-}\Delta_t \\ -\frac{\partial \Omega_{bb}}{\partial \bar{u}_n^+}\Delta_b & -\frac{\partial \Omega_{bb}}{\partial \bar{u}_t^+}\Delta_b & -\frac{\partial \Omega_{bb}}{\partial \bar{u}_b^+}\Delta_b & \frac{\partial \Omega_{bb}}{\partial \bar{u}_n^-}\Delta_b & \frac{\partial \Omega_{bb}}{\partial \bar{u}_t^-}\Delta_b & \frac{\partial \Omega_{bb}}{\partial \bar{u}_b^-}\Delta_b \\ \frac{\partial \Omega_{nn}}{\partial \bar{u}_n^+}\Delta_n & \frac{\partial \Omega_{nn}}{\partial \bar{u}_t^+}\Delta_n & \frac{\partial \Omega_{nn}}{\partial \bar{u}_b^+}\Delta_n & -\frac{\partial \Omega_{nn}}{\partial \bar{u}_n^-}\Delta_n & -\frac{\partial \Omega_{nn}}{\partial \bar{u}_t^-}\Delta_n & -\frac{\partial \Omega_{nn}}{\partial \bar{u}_b^-}\Delta_n \\ \frac{\partial \Omega_{tt}}{\partial \bar{u}_n^+}\Delta_t & \frac{\partial \Omega_{tt}}{\partial \bar{u}_t^+}\Delta_t & \frac{\partial \Omega_{tt}}{\partial \bar{u}_b^+}\Delta_t & -\frac{\partial \Omega_{tt}}{\partial \bar{u}_n^-}\Delta_t & -\frac{\partial \Omega_{tt}}{\partial \bar{u}_t^-}\Delta_t & -\frac{\partial \Omega_{tt}}{\partial \bar{u}_b^-}\Delta_t \\ \frac{\partial \Omega_{bb}}{\partial \bar{u}_n^+}\Delta_b & \frac{\partial \Omega_{bb}}{\partial \bar{u}_t^+}\Delta_b & \frac{\partial \Omega_{bb}}{\partial \bar{u}_b^+}\Delta_b & -\frac{\partial \Omega_{bb}}{\partial \bar{u}_n^-}\Delta_b & -\frac{\partial \Omega_{bb}}{\partial \bar{u}_t^-}\Delta_b & -\frac{\partial \Omega_{bb}}{\partial \bar{u}_b^-}\Delta_b \end{bmatrix}^{n(j)} . \tag{3.7-12}$$

3.8 Weak Coupling

The traction-separation-models used depend on the current damage state $\omega_{(n)}$:

$$\bar{\mathbf{t}}_{(n)}^{n(j)} = \mathbf{\Omega}^{n(j)}(\omega_{(n)}^{n(j)}) \cdot \bar{\mathbf{\Delta}}_{(n)}^{n(j)} , \tag{3.8-1}$$

where the evolution of the damage variable $\omega_{(n)}^{n(j)}$ is a function of the current surface-averaged displacement-discontinuity:

$$\omega_{(n)}^{n(j)} = f(\bar{\mathbf{\Delta}}_{(n)}^{n(j)}) . \tag{3.8-2}$$

This relations shown in Eq. (3.8-1) and (3.8-2) between tractions, displacement jump and damage variable is called “strong coupling” that leads to the nonlinear system of equations (3.5-9). Another way is to use the previous damage state $\omega_{(n-1)}$ in the traction-separation-law, called “weak coupling”:

$$\bar{\mathbf{t}}_{(n)}^{n(j)} = \mathbf{\Omega}^{n(j)}(\omega_{(n-1)}^{n(j)}) \cdot \bar{\mathbf{\Delta}}_{(n)}^{n(j)} \tag{3.8-3}$$

and update it after solving the microstructure system of equations, which is linear:

$$\left[\widehat{\mathbf{K}} - \widehat{\mathbf{I}}(\boldsymbol{\omega}_{(n)})\right] \bar{\mathbf{r}}'_{(n+1)} = -\widehat{\mathbf{D}}\boldsymbol{\varepsilon}^0_{(n+1)} . \tag{3.8-4}$$

The advantage of this method is the overall system of equations is linear, i. e. no linearization is necessary and convergence problems can not occur. On the other hand, the accuracy of the solution depends on the macro step size.

3.9 Parameter Studies

In order to verify the implementation and study the behavior of the used tractions-separation-laws, a sandwich-test is used , which consists of two solid-subcells embedding an interface-subcell, see Fig 3.9-2. The basic interface parameters chosen for the parameters studies with the three different traction-separation-laws are presented in Tab. 3.9-1.

Fig. 3.9-1: Chosen interface parameters

Parameter	Value
normal strength $\hat{t}_n$ [MPa]	50
shear strength $\hat{t}_\tau$ [MPa]	25
normal failure displacement jump $\hat{\Delta}_n$ [μm]	0.05
shear failure displacement jump $\hat{\Delta}_\tau$ [μm]	0.025

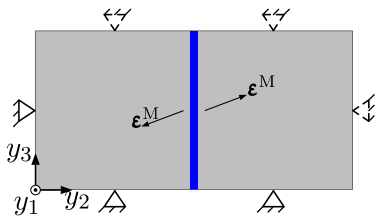

Fig. 3.9-2: Sandwich-test

Consistent linearization vs. weak-coupling

Fig. 3.9-3 shows the results for a consistent linearization of the nonlinear system of equations and for a weak-coupling at the subcell-level under a macro strain ϵ^0_{22}. As expected, the difference between the numerically exact solution and the weak-coupling one depends on the used macro step size $\Delta\epsilon^0_{22}$. A very small step size ($\Delta\epsilon^0_{22} = 10^{-6}$) must be chosen to minimize the deviation.

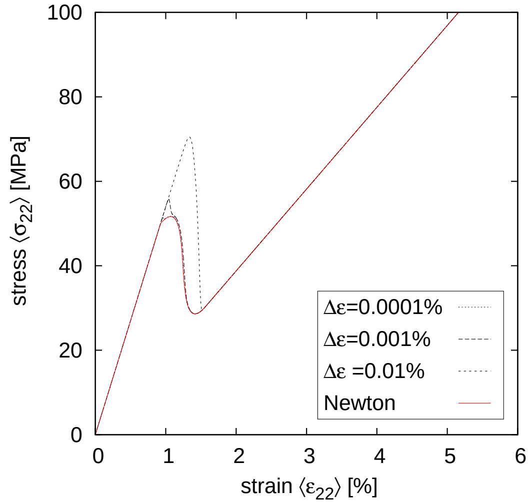

Fig. 3.9-3: Comparison between weak coupling and consistent linearization

Chaboche

Fig. 3.9-4 illustrates the influence of varying the failure displacement jump Δ_{nf} on the effective stress-strain-curve by using Chaboche's model. This variation affects the entire macroscopic course including strength and softening area. The smaller the failure displacement jump the steeper the decrease after reaching the maximum stress. A failure displacement jump of $\Delta_{\mathrm{nf}} = 0.02\,\mu$m leads to loss of convergence of Newton's method at the maximum point. The stress increase after its drop is caused by the bearing.

Lissenden

The parameter study by using Lissenden's model and varying the failure displacement jump is presented in Fig. 3.9-5 (a). The effective stress-strain-curve is the same for all parameter sets up to reaching the stress criterion (3.4-14). Afterwards, the macroscopic behavior differs heavily. The iteration process stops at the stress criterion for the smallest chosen failure parameter again. The stress increases after the softening area because of the bearing.

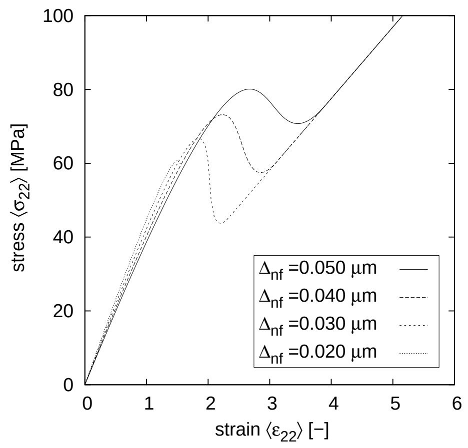

Fig. 3.9-4: Traction-separation-model by Chaboche: effective stress-strain-curve $\langle\sigma_{22}\rangle$-$\langle\varepsilon_{22}\rangle$ for different prescribed failure displacement jumps

Camanho and Davila

Fig. 3.9-5 (b) shows the effective stress-strain-curve created by the use of Camanho and Davila's model for the interface-subcell on the microscopic level. The linear-softening area of this model is clearly visible in the macroscopic answer. Again, the smallest chosen failure displacement jump leads to loss of convergence of Newton's method and the stress increase is caused by the bearing.

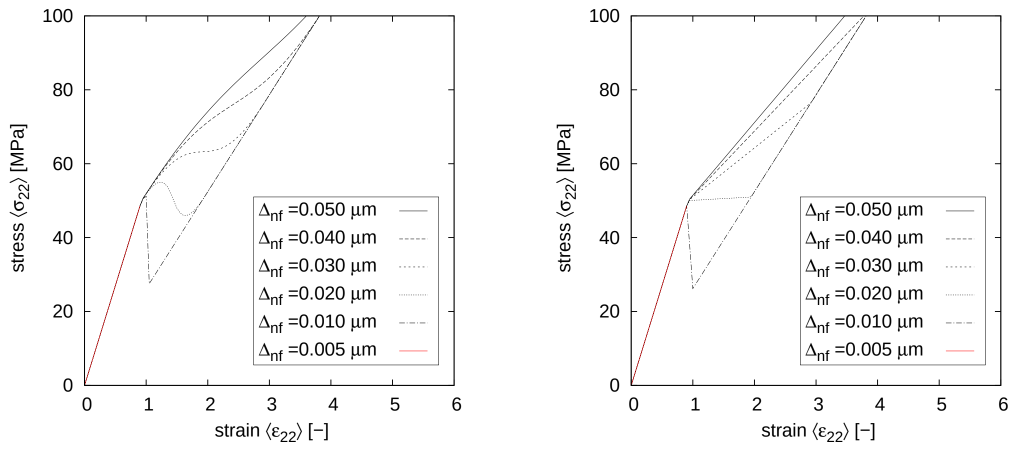

Fig. 3.9-5: Effective stress-strain-curve $\langle\sigma_{22}\rangle$-$\langle\varepsilon_{22}\rangle$ for different prescribed failure displacement jumps (a) Traction-separation-model by Lissenden (b) Traction-separation-model by Camanho und Davila

4 Extended Finite-Element-Method (X-FEM)

M. Donhauser, M. Schmerbauch, A. Matzenmiller

In a multiscale analysis the HFGMC with cohesive interface damage provides the effective material stiffness at each GAUSSian point. The damage evolution at the micro scale leads at a critical damage state to crack initiation at the macro scale. The crack is then taken into account mesh independent using the extended finite element method. The critical damage state ω_c where the crack initiates can be defined by:

- the damaged state where failure of the RUC occurs, see Fig. 4.0-1 (a)

or

- the point of stress maximum before the softening range, see Fig. 4.0-1 (b).

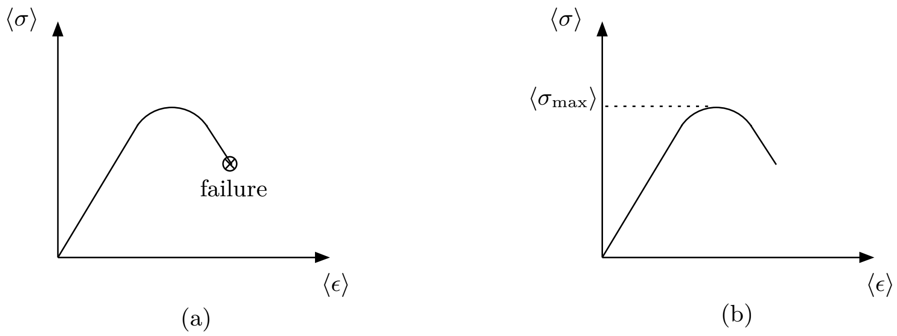

Fig. 4.0-1: Effective stress-strain-curve of an arbitrary Gaussian point with macro crack initiation criterion: (a) point of failure (b) stress maximum

4.1 Spatial Discretization

The Extended Finite-Element-Method (XFEM) firstly published in [6] and [23] is a numerical method of calculation, which enables a mesh-independent representation of discontinuities such as cracks in a finite element model. The fundamental difference to the classical Finite-Element-Method (FEM) is an enhanced displacement approach. In the X-FEM the displacement field approach $\mathbf{u}^{\mathrm{h}}$ is composed of a standard part corresponding to the classical FEM and an enrichment part that takes the discontinuity into account:

$$\mathbf{u}^{\mathrm{h}}(\mathbf{x}) = \underbrace{\sum_{i \in \mathcal{S}} N_i(\mathbf{x}) \mathbf{u}_i}_{\text{standard}} + \underbrace{\sum_{j \in \mathcal{S}_c} N_j(\mathbf{x}) \psi \mathbf{a}_j}_{\text{enrichment}} \; , \tag{4.1-1}$$

where $\mathbf{x}$ stands for the global position vector, N_i and N_j for isoparametric shape functions, $\mathbf{u}_i$ for the unknown nodal displacements, ψ for the enrichment function of the discontinuity and $\mathbf{a}_j$ for the additional unknowns due to the enrichment. The set $\mathcal{S}$ includes all nodes of the finite-element model and the set $\mathcal{S}_c$ only those which should be enriched additionally. The following enhanced approach captures the problem of a crack (strong discontinuity) in a two-dimensional FE-model:

$$\mathbf{u}^{\mathrm{h}}(\mathbf{x}) = \sum_{i \in \mathcal{S}} N_i(\mathbf{x})\mathbf{u}_i + \sum_{j \in \mathcal{S}_{\mathrm{CTE}}} N_j(\mathbf{x}) \Big[\sum_{k=1}^{4} \Big(F^k(\mathbf{x}) - F^k(\mathbf{x}_j) \Big) \mathbf{b}_j^k \Big] + \sum_{l \in \mathcal{S}_{\mathrm{CE}}} N_l(\mathbf{x}) \Big(H(\mathbf{x}) - H(\mathbf{x}_l) \Big) \mathbf{a}_l \tag{4.1-2}$$

where the enrichment functions F^k represent the singularity at the crack tip and the Heaviside function H the jump of the displacement field because of the crack. For classification, a plate with an inclined crack and the discretized XFEM-model is illustrated in Fig. 4.1-1 (a)-(b). The discretized FE-model consists of four different element types as shown in Fig. 4.1-1 (b). The element nodes surrounded by a blue box belongs to the set $\mathcal{S}_{\mathrm{CTE}}$ and are enriched by the crack tip functions F_k as well as the nodes surrounded by an orange box belongs to the set $\mathcal{S}_{\mathrm{CE}}$ and are enriched by the Heaviside function H.

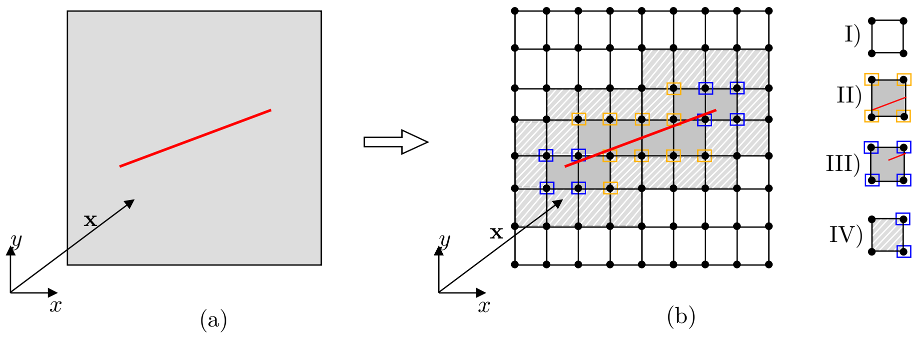

Fig. 4.1-1: (a): Plate with an inclined crack, (b): Discretized XFEM-model with different element types I) solid element, II) cut element, III) crack tip element, IV) blending element

4.2 Element Stiffness

Cut element

A crack visualized by a solid line separates a two-dimensional cut element into two parts (domain Ω^+ and Ω^-), having 16 element degrees of freedom (DOF), 8 due to the classical displacement approach and 8 due to the enrichment, see Fig. 4.2-1. The Heaviside function is used to represent the jump in the displacement field across the crack in the entire element. Thus, the displacement approach at the element level is given by:

$$\mathbf{u}^{\mathrm{e}}(\mathbf{x}) = \sum_{i=1}^{4} N_i \mathbf{u}_i + \sum_{i=1}^{4} \underbrace{N_i \Big(H(\mathbf{x}) - H(\mathbf{x}_i) \Big)}_{\Psi_i} \mathbf{a}_i \; . \tag{4.2-1}$$

The isoparametric shape functions N_i are defined in the natural coordinates (ξ, η) as follows:

$$N_1 = \frac{1}{4}(1-\xi)(1-\eta) \qquad N_2 = \frac{1}{4}(1+\xi)(1-\eta) \tag{4.2-2}$$

$$N_3 = \frac{1}{4}(1+\xi)(1+\eta) \qquad N_4 = \frac{1}{4}(1-\xi)(1+\eta) \tag{4.2-3}$$

as well as the Heaviside function H:

$$H(\mathbf{x}) = +1 \quad \forall \mathbf{x} \in \ \Omega^+ \tag{4.2-4}$$

$$H(\mathbf{x}) = -1 \quad \forall \mathbf{x} \in \ \Omega^- \ , \tag{4.2-5}$$

where Ω^+ is the upper and Ω^- lower domain, see Fig. 4.2-1. The displacement approach (4.2-1) is written in matrix notation

$$\mathbf{u}^{\mathrm{e}} = \underbrace{\begin{bmatrix} N_1 & 0 & N_2 & 0 & N_3 & 0 & N_4 & 0 \\ 0 & N_1 & 0 & N_2 & 0 & N_3 & 0 & N_4 \end{bmatrix}}_{\mathbf{N}^{\mathrm{Std}}} \underbrace{\begin{bmatrix} u_1 \\ v_1 \\ \vdots \\ u_4 \\ v_4 \end{bmatrix}}_{\mathbf{u}} + \underbrace{\begin{bmatrix} \Psi_1 & 0 & \Psi_2 & 0 & \Psi_3 & 0 & \Psi_4 & 0 \\ 0 & \Psi_1 & 0 & \Psi_2 & 0 & \Psi_3 & 0 & \Psi_4 \end{bmatrix}}_{\mathbf{N}^{\mathrm{Enr}}} \underbrace{\begin{bmatrix} a_{1x} \\ a_{1y} \\ \vdots \\ a_{4x} \\ a_{4y} \end{bmatrix}}_{\mathbf{a}} \tag{4.2-6}$$

$$\mathbf{u}^{\mathrm{e}} = \begin{bmatrix} \mathbf{N}^{\mathrm{Std}} & \mathbf{N}^{\mathrm{Enr}} \end{bmatrix} \begin{bmatrix} \mathbf{u} \\ \mathbf{a} \end{bmatrix}, \tag{4.2-7}$$

where $\mathbf{N}^{\mathrm{Std}}$ stands for the "shape function matrix" and $\mathbf{N}^{\mathrm{Enr}}$ for the "enrichment function matrix". The strain tensor is given by

$$\boldsymbol{\varepsilon} = \begin{bmatrix} \varepsilon_{11} \\ \varepsilon_{22} \\ \varepsilon_{12} \end{bmatrix} = \underbrace{\begin{bmatrix} \frac{\partial}{\partial x} & 0 \\ 0 & \frac{\partial}{\partial y} \\ \frac{\partial}{\partial y} & \frac{\partial}{\partial x} \end{bmatrix}}_{\mathbf{D}} \begin{bmatrix} u \\ v \end{bmatrix} , \tag{4.2-8}$$

where $\mathbf{D}$ is the differential-operator and (u, v) the displacement field. Applying Eq. (4.2-8) to

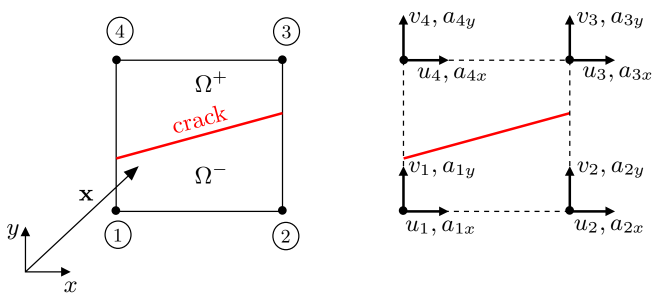

Fig. 4.2-1: Cut element with nodal degrees of freedom

the displacement field (4.2-7), the approximated strain tensor becomes

$$\boldsymbol{\epsilon}^{\mathrm{e}} = \begin{bmatrix} \mathbf{B}^{\mathrm{Std}} & \mathbf{B}^{\mathrm{Enr}} \end{bmatrix} \begin{bmatrix} \mathbf{u} \\ \mathbf{a} \end{bmatrix} = \tilde{\mathbf{B}} \tilde{\mathbf{u}} \tag{4.2-9}$$

with the operators

$$\mathbf{B}^{\mathrm{Std}} = \mathbf{D}\mathbf{N} = \begin{bmatrix} N_{1,x} & 0 & N_{2,x} & 0 & N_{3,x} & 0 & N_{4,x} & 0 \\ 0 & N_{1,y} & 0 & N_{2,y} & 0 & N_{3,y} & 0 & N_{4,y} \\ N_{1,y} & N_{1,x} & N_{2,y} & N_{2,x} & N_{3,y} & N_{2,x} & N_{4,y} & N_{4,x} \end{bmatrix} \tag{4.2-10}$$

$$\mathbf{B}^{\mathrm{Enr}} = \mathbf{D}\boldsymbol{\Psi} = \begin{bmatrix} \Psi_{1,x} & 0 & \Psi_{2,x} & 0 & \Psi_{3,x} & 0 & \Psi_{4,x} & 0 \\ 0 & \Psi_{1,y} & 0 & \Psi_{2,y} & 0 & \Psi_{3,y} & 0 & \Psi_{4,y} \\ \Psi_{1,y} & \Psi_{1,x} & \Psi_{2,y} & \Psi_{2,x} & \Psi_{3,y} & \Psi_{2,x} & \Psi_{4,y} & \Psi_{4,x} \end{bmatrix} . \tag{4.2-11}$$

The derivation of the isoparametric shape functions are:

$$N_{i,x} = \frac{\partial N_i}{\partial \xi}\frac{\partial \xi}{\partial x} + \frac{\partial N_i}{\partial \eta}\frac{\partial \eta}{\partial x} \qquad N_{i,y} = \frac{\partial N_i}{\partial \xi}\frac{\partial \xi}{\partial y} + \frac{\partial N_i}{\partial \eta}\frac{\partial \eta}{\partial y} \tag{4.2-12}$$

and of the enrichment functions:

$$\Psi_{i,x} = N_{i,x}\left(H(\mathbf{x}) - H(\mathbf{x_i})\right) \qquad \Psi_{i,y} = N_{i,y}\left(H(\mathbf{x}) - H(\mathbf{x_i})\right) \tag{4.2-13}$$

with

$$H(\mathbf{x})_{,x} = \begin{cases} 1 & \text{at crack} \\ 0 & \text{else} \end{cases} . \tag{4.2-14}$$

Assuming linear-elastic material behavior

$$\boldsymbol{\sigma} = \mathbf{C}\boldsymbol{\epsilon} \ , \tag{4.2-15}$$

where $\mathbf{C}$ denotes the fourth order elasticity tensor. The internal virtual work δA^e_{int} at the element level

$$\delta A^{\mathrm{e}}_{\text{int}} = \int_{\Omega_e} \delta\boldsymbol{\epsilon} : \boldsymbol{\sigma} \, \mathrm{d}\Omega \ , \tag{4.2-16}$$

becomes

$$\delta A^{\mathrm{e}}_{\text{int}} = \delta\tilde{\mathbf{u}}^{\mathsf{T}}_{\mathrm{e}} \underbrace{\int_{\Omega_{\mathrm{e}}} \tilde{\mathbf{B}}^{\mathsf{T}}\mathbf{C}\tilde{\mathbf{B}} \, \mathrm{d}\Omega}_{\mathbf{k}^{\mathrm{e}}} \tilde{\mathbf{u}}_{\mathrm{e}} \qquad \text{with} \qquad \tilde{\mathbf{B}} = \begin{bmatrix}\mathbf{B}^{\text{Std}} & \mathbf{B}^{\text{Enr}}\end{bmatrix} \tag{4.2-17}$$

by using the strain tensor (4.2-9) and the constitutive model (4.2-15). The integral term in Eq. (4.2-17) is the stiffness matrix $\mathbf{k}^{\mathrm{e}}$ with $\mathbf{k}^{\mathrm{e}} \in \mathbb{R}^{16\times16}$ of the cut element:

$$\mathbf{k}^{\mathrm{e}} = \int_{\Omega_{\mathrm{e}}} \tilde{\mathbf{B}}^{\mathsf{T}}\mathbf{C}\tilde{\mathbf{B}}\mathrm{d}\Omega \tag{4.2-18}$$

$$= \begin{bmatrix} \int_{\Omega_{\mathrm{e}}} \mathbf{B}^{\text{Std}^{\mathsf{T}}}\mathbf{C}\mathbf{B}^{\text{Std}}\mathrm{d}\Omega & \int_{\Omega_{\mathrm{e}}} \mathbf{B}^{\text{Std}^{\mathsf{T}}}\mathbf{C}\mathbf{B}^{\text{Enr}}\mathrm{d}\Omega \\ \int_{\Omega_{\mathrm{e}}} \mathbf{B}^{\text{Enr}^{\mathsf{T}}}\mathbf{C}\mathbf{B}^{\text{Std}}\mathrm{d}\Omega & \int_{\Omega_{\mathrm{e}}} \mathbf{B}^{\text{Enr}^{\mathsf{T}}}\mathbf{C}\mathbf{B}^{\text{Enr}}\mathrm{d}\Omega \end{bmatrix} = \begin{bmatrix} \mathbf{k}_{11} & \mathbf{k}_{12} \\ \mathbf{k}_{21} & \mathbf{k}_{22} \end{bmatrix} . \tag{4.2-19}$$

Since the Heaviside function is contained in the matrices $\mathbf{k}_{12}$ and $\mathbf{k}_{21}$, the integrand is not continuous over the integration domain. To evaluate the integrals of these sub-stiffness matrices, a subdivision of the integration domain is necessary, see for instance [12] and [13].

Crack tip element

This element type contains the crack tip and is only cut in a defined area, see Fig. 4.2-2. The displacement field is solely discontinuous across the crack. Moreover, the enrichment functions must be able to represent the stress singularity at the crack tip. Parts of the analytical solution given by the linear elastic fracture mechanics (LEFM) for linear elastic and isotropic materials have these properties and are used to create the enrichment functions of the crack tip element, see [6]:

$$F^1(r,\theta) = \sqrt{r}\,\sin\Big(\frac{\theta}{2}\Big) \tag{4.2-20}$$

$$F^2(r,\theta) = \sqrt{r}\,\cos\Big(\frac{\theta}{2}\Big) \tag{4.2-21}$$

$$F^3(r,\theta) = \sqrt{r}\,\sin\Big(\frac{\theta}{2}\Big)\sin(\theta) \tag{4.2-22}$$

$$F^4(r,\theta) = \sqrt{r}\,\cos\Big(\frac{\theta}{2}\Big)\sin(\theta)\ . \tag{4.2-23}$$

The enrichment functions F^1, F^2, F^3 and F^4 are defined in a polar coordinate system (r,θ) at the crack tip, see Fig. 4.2-2. The element has 40 degrees of freedom, 8 nodal displacements $\mathbf{u}_i$ and additional 32 unknowns $\mathbf{b}_j^k$ by the enrichment. Hence, the displacement approach at the element level reads as follows:

$$\mathbf{u}^{\mathrm{e}}(\mathbf{x}) = \sum_{i=1}^{4} N_i \mathbf{u}_i + \sum_{j=1}^{4} N_j \Bigg(\sum_{k=1}^{4}\Big(F^k(\mathbf{x}) - F^k(\mathbf{x}_j)\Big)\Bigg)\mathbf{b}_j^k \tag{4.2-24}$$

or in matrix-vector notation

$$\mathbf{u}^{\mathrm{e}}(\mathbf{x}) = [\mathbf{N}_1 \quad \mathbf{N}_2 \quad \mathbf{N}_3 \quad \mathbf{N}_4 \quad \boldsymbol{\Phi}_1 \quad \boldsymbol{\Phi}_2 \quad \boldsymbol{\Phi}_3 \quad \boldsymbol{\Phi}_4] \begin{bmatrix} \mathbf{u}_1 \\ \mathbf{u}_2 \\ \mathbf{u}_3 \\ \mathbf{u}_4 \\ \mathbf{b}_1 \\ \mathbf{b}_2 \\ \mathbf{b}_3 \\ \mathbf{b}_4 \end{bmatrix}\ , \tag{4.2-25}$$

with the sub-matrices of the shape functions $\mathbf{N}_i$, of the enrichment functions $\boldsymbol{\Phi}_i$ and the sub-vectors at node i:

$$\mathbf{N}_i = \begin{bmatrix} N_i & 0 \\ 0 & N_i \end{bmatrix}\ , \qquad \mathbf{u}_i = \begin{bmatrix} u_i \\ v_i \end{bmatrix}\ , \tag{4.2-26}$$

$$\boldsymbol{\Phi}_i = \begin{bmatrix} F_i^1 & 0 & F_i^2 & 0 & F_i^3 & 0 & F_i^4 & 0 \\ 0 & F_i^1 & 0 & F_i^2 & 0 & F_i^3 & 0 & F_i^4 \end{bmatrix}\ , \tag{4.2-27}$$

$$\mathbf{b}_i = \Big[b_{ix}^1 \quad b_{iy}^1 \quad b_{ix}^2 \quad b_{iy}^2 \quad b_{ix}^3 \quad b_{iy}^3 \quad b_{ix}^4 \quad b_{iy}^4\Big]^{\mathsf{T}}\ . \tag{4.2-28}$$

Using Eq. (4.2-8) and Eq. (4.2-25) the strain at the element level is obtained:

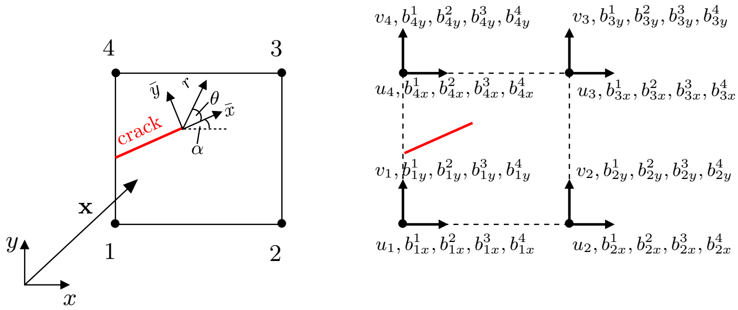

Fig. 4.2-2: Crack tip element with nodal degrees of freedom and local Cartesian $(\bar{x}, \bar{y})$ and polar coordinate system (r, θ) at the crack tip

$$\boldsymbol{\varepsilon}^{\mathrm{e}} = \underbrace{\left[\overbrace{\mathbf{B}_1^{\mathrm{Std}} \quad \mathbf{B}_2^{\mathrm{Std}} \quad \mathbf{B}_3^{\mathrm{Std}} \quad \mathbf{B}_4^{\mathrm{Std}}}^{\mathbf{B}^{\mathrm{Std}}} \overbrace{\mathbf{B}_1^{\mathrm{CT}} \quad \mathbf{B}_2^{\mathrm{CT}} \quad \mathbf{B}_3^{\mathrm{CT}} \quad \mathbf{B}_4^{\mathrm{CT}}}^{\mathbf{B}^{\mathrm{CT}}}\right]}_{\hat{\mathbf{B}}} \underbrace{\begin{bmatrix} \mathbf{u}_1 \\ \mathbf{u}_2 \\ \mathbf{u}_3 \\ \mathbf{u}_4 \\ \mathbf{b}_1 \\ \mathbf{b}_2 \\ \mathbf{b}_3 \\ \mathbf{b}_4 \end{bmatrix}}_{\hat{\mathbf{u}}} = \hat{\mathbf{B}}\hat{\mathbf{u}} \tag{4.2-29}$$

with the corresponding operators

$$\mathbf{B}_i^{\mathrm{Std}} = \begin{bmatrix} N_{i,x} & 0 \\ 0 & N_{i,y} \\ N_{i,y} & N_{i,x} \end{bmatrix} \quad \mathbf{B}_i^{\mathrm{CT}} = \begin{bmatrix} F^1_{i,x} & 0 & F^2_{i,x} & 0 & F^3_{i,x} & 0 & F^4_{i,x} & 0 \\ 0 & F^1_{i,y} & 0 & F^2_{i,y} & 0 & F^3_{i,y} & 0 & F^4_{i,y} \\ F^1_{i,y} & F^1_{i,x} & F^2_{i,y} & F^2_{i,x} & F^3_{i,y} & F^3_{i,x} & F^4_{i,y} & F^4_{i,x} \end{bmatrix} \tag{4.2-30}$$

and derivations

$$F^k_{i,x} = N_{i,x}(F^k(\mathbf{x}) - F^k(\mathbf{x}_i)) + N_i F^k_{,x} \tag{4.2-31}$$

$$F^k_{i,y} = N_{i,y}(F^k(\mathbf{x}) - F^k(\mathbf{x}_i)) + N_i F^k_{,y} \; . \tag{4.2-32}$$

The derivations of the crack tip enrichment functions $F^k_{,x}$ and $F^k_{,y}$ are calculated by the relation between the global coordinate system (x, y) and the local coordinate systems at the crack tip and using the chain rule twice, see for details [17]:

$$F^1_{,x} = -\frac{1}{2\sqrt{r}}\sin\left(\frac{\theta}{2}\right)\cos(\alpha) - \frac{1}{2\sqrt{r}}\cos\left(\frac{\theta}{2}\right)\sin(\alpha) \tag{4.2-33}$$

$$F^2_{,x} = \frac{1}{2\sqrt{r}}\cos\left(\frac{\theta}{2}\right)\cos(\alpha) - \frac{1}{2\sqrt{r}}\sin\left(\frac{\theta}{2}\right)\sin(\alpha) \tag{4.2-34}$$

$$F^3_{,x} = -\frac{1}{2\sqrt{r}}\sin\left(\frac{3\theta}{2}\right)\sin(\theta)\cos(\alpha) - \frac{1}{2\sqrt{r}}\left(\sin\left(\frac{\theta}{2}\right) + \sin\left(\frac{3\theta}{2}\right)\cos(\theta)\right)\sin(\alpha) \tag{4.2-35}$$

$$F^4_{,x} = -\frac{1}{2\sqrt{r}}\cos\left(\frac{3\theta}{2}\right)\sin(\theta)\cos(\alpha) - \frac{1}{2\sqrt{r}}\left(\cos\left(\frac{\theta}{2}\right) + \cos\left(\frac{3\theta}{2}\right)\cos(\theta)\right)\sin(\alpha) \tag{4.2-36}$$

$$F^1_{,y} = -\frac{1}{2\sqrt{r}}\sin\left(\frac{\theta}{2}\right)\sin(\alpha) + \frac{1}{2\sqrt{r}}\cos\left(\frac{\theta}{2}\right)\cos(\alpha) \tag{4.2-37}$$

$$F^2_{,y} = \frac{1}{2\sqrt{r}}\cos\left(\frac{\theta}{2}\right)\sin(\alpha) + \frac{1}{2\sqrt{r}}\sin\left(\frac{\theta}{2}\right)\cos(\alpha) \tag{4.2-38}$$

$$F^3_{,y} = -\frac{1}{2\sqrt{r}}\sin\left(\frac{3\theta}{2}\right)\sin(\theta)\sin(\alpha) + \frac{1}{2\sqrt{r}}\left(\sin\left(\frac{\theta}{2}\right) + \sin\left(\frac{3\theta}{2}\right)\cos(\theta)\right)\cos(\alpha) \tag{4.2-39}$$

$$F^4_{,y} = -\frac{1}{2\sqrt{r}}\cos\left(\frac{3\theta}{2}\right)\sin(\theta)\sin(\alpha) + \frac{1}{2\sqrt{r}}\left(\cos\left(\frac{\theta}{2}\right) + \cos\left(\frac{3\theta}{2}\right)\cos(\theta)\right)\cos(\alpha)\ . \tag{4.2-40}$$

Using Eq. (4.2-29) and Eq. (4.2-16), the virtual work of the element level becomes:

$$\delta A^{\mathrm{e}}_{\mathrm{int}} = \delta\hat{\mathbf{u}}^{\mathsf{T}}_{\mathrm{e}} \underbrace{\int_{\Omega_{\mathrm{e}}} \hat{\mathbf{B}}^{\mathsf{T}}\mathbf{C}\hat{\mathbf{B}}\mathrm{d}\Omega}_{\mathbf{k}^{\mathrm{e}}}\ \hat{\mathbf{u}}_{\mathrm{e}} \qquad \text{with} \qquad \hat{\mathbf{B}} = \begin{bmatrix}\mathbf{B}^{\mathrm{Std}} & \mathbf{B}^{\mathrm{CT}}\end{bmatrix}\ , \tag{4.2-41}$$

where the integral term denotes the element stiffness matrix of the crack tip element

$$\mathbf{k}^e = \int_{\Omega_e} \hat{\mathbf{B}}^{\mathsf{T}}\mathbf{C}\hat{\mathbf{B}}\,\mathrm{d}\Omega \tag{4.2-42}$$

$$= \begin{bmatrix} \int_{\Omega_e} \mathbf{B}^{\mathrm{Std}^{\mathsf{T}}}\mathbf{C}\mathbf{B}^{\mathrm{Std}}\mathrm{d}\Omega & \int_{\Omega_e} \mathbf{B}^{\mathrm{Std}^{\mathsf{T}}}\mathbf{C}\mathbf{B}^{\mathrm{CT}}\mathrm{d}\Omega \\ \int_{\Omega_e} \mathbf{B}^{\mathrm{CT}^{\mathsf{T}}}\mathbf{C}\mathbf{B}^{\mathrm{Std}}\mathrm{d}\Omega & \int_{\Omega_e} \mathbf{B}^{\mathrm{CT}^{\mathsf{T}}}\mathbf{C}\mathbf{B}^{\mathrm{CT}}\mathrm{d}\Omega \end{bmatrix} = \begin{bmatrix} \mathbf{k}_{11} & \mathbf{k}_{12} \\ \mathbf{k}_{21} & \mathbf{k}_{22} \end{bmatrix} \qquad \mathbf{k}^e \in \mathbb{R}^{40\times 40}\ . \tag{4.2-43}$$

Because of the trigonometric functions and the $\sqrt{r}$ singularity in the derivations of the enrichment functions, see Eqs. (4.2-33) - (4.2-40), the evaluation of the integrals of the stiffness matrix with the standard Gaussian quadrature leads to inaccurate results. Thus, the crack tip element is subdivided into sub-triangles for the integration procedure and each domain is integrated by the "almost polar integration method" proposed by [20] to achieve accurate results.

4.3 Multiscale Analysis

The finite-element program FEAP [26] in its version 8.2 is used to implement the Extended Finite-Element-Method, presented in the previous sections. So, the cut element, crack tip element and blending element are programmed as user elements. In a first step, the linear-elastic HFGMC is employed as user material model in the finite element program FEAP. The extended finite

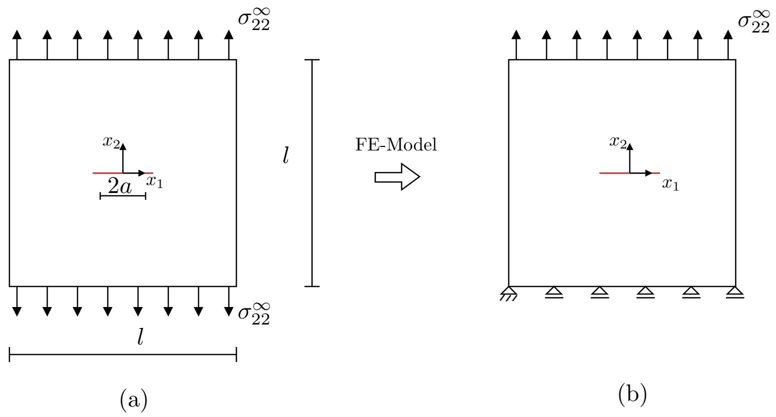

Fig. 4.3-1: (a): Plate under tensile load with crack (red) inside, (b): FE-model of the plate with applied boundary conditions

element routines are modified in such a way that the HFGMC is called at each GAUSSian point and provides the necessary effective stiffness. A coupled simulation is conducted of a "infinite" plate under tensile load (Mode-I) with a central straight crack inside, see Fig. 4.3-1, to verify the implementation and compare the results to analytical ones. Since isotropic enrichment functions (4.2-20) - (4.2-23) are used, the material parameters of the HFGMC are chosen to represent isotropic material behavior at the microscale. The square plate has the following dimensions and material parameters

- length: $l = 30\,\mathrm{mm}$
- bulk modulus $\mathrm{K} = 175000\,\mathrm{MPa}$
- shear modulus $\mathrm{G} = 80769\,\mathrm{MPa}$.

The crack length is $2a = 2\,\mathrm{mm}$ and the applied tensile load is $\sigma_{22}^{\infty} = 100\,\mathrm{MPa}$. The plate is discretized with $61 \times 63 = 3843$ finite elements in plane stress. A part of the deformed mesh configuration is shown in Fig. 4.3-2 (a). The enriched element around the crack can represent the deformation expected because the mesh distort in the area. Fig. 4.3-2 (b) shows the simulation results of the predicted stress distribution in load direction. The highest stress values are in front of the crack tip. The theoretical solution shows the same results, which has a stress singularity there. This result corresponds to the theoretical solution which has an singularity in the stress field at the crack tip. The stress has the lowest values in the centre of the crack, where the gap is visible. The stress distribution reaches the applied boundary magnitude in a sufficient distance from the crack and its tip, respectively. It is possible to consider in the multiscale analysis the stress distribution in the RUC at the micro scale. The area in front of the crack tip is the most important region in that case. Because of the symmetry of the problem (geometry and load application), it is sufficient to consider only one crack tip, here the right crack tip is chosen, see Fig. 4.3-3 (a). The analytical solution of the stress field in front of the crack tip ($x_1 \geq 0$ and

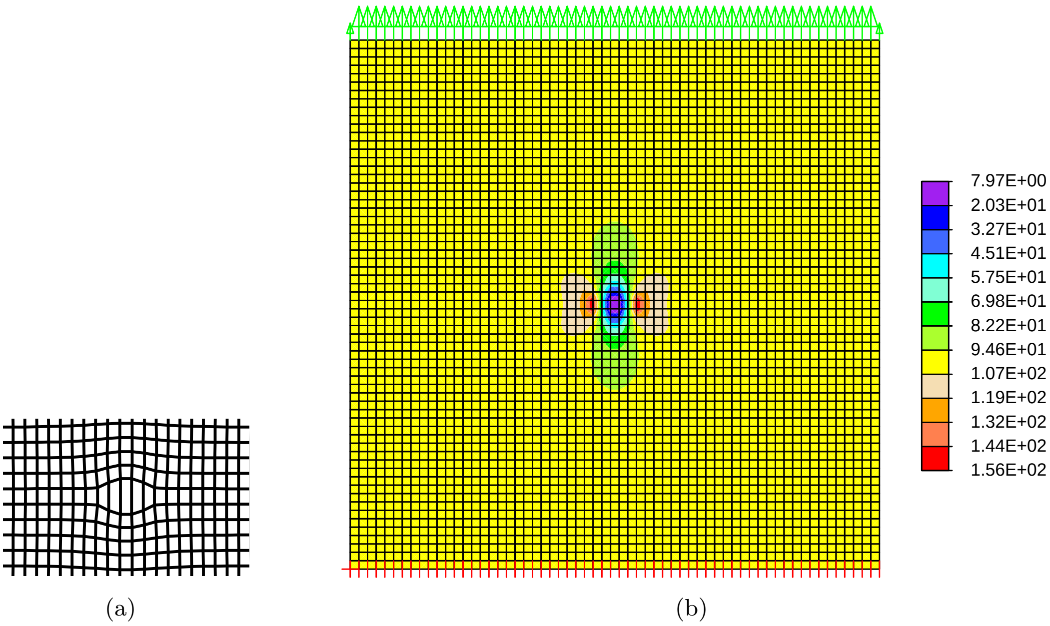

Fig. 4.3-2: (a): Part of the deformed mesh configuration magnified 500 times, (b):Contour plot of the stress distribution σ_{22} for the plate with interior crack at the macro scale

x_2=0) is given by [18]:

$$\sigma_{22} = \sigma_{22}^{\infty} \frac{x_1}{a\sqrt{(x_1/a)^2 - 1}} \,, \tag{4.3-1}$$

where a is the half crack length and x_1 denotes the axis. In Fig. 4.3-3 (b), the predicted stress values at the Gaussian points in front of the crack tip as well as the analytical solution of the stress field (4.3-1) are depicted. Furthermore, the stress distribution in the RUC is visible for certain GAUSSian points, which is homogenous since a homogenous microstructure is considered. The largest numerical stress value and its deviation to the analytical solution is obtained at the closest GAUSSian point with the shortest distance to the crack tip (x_1 =0.01 mm). The deviation between numerical and analytical solution declines with increasing distance from the crack tip. These first results show the HFGMC and the XFEM are implemented correct and the multiscale analysis works.

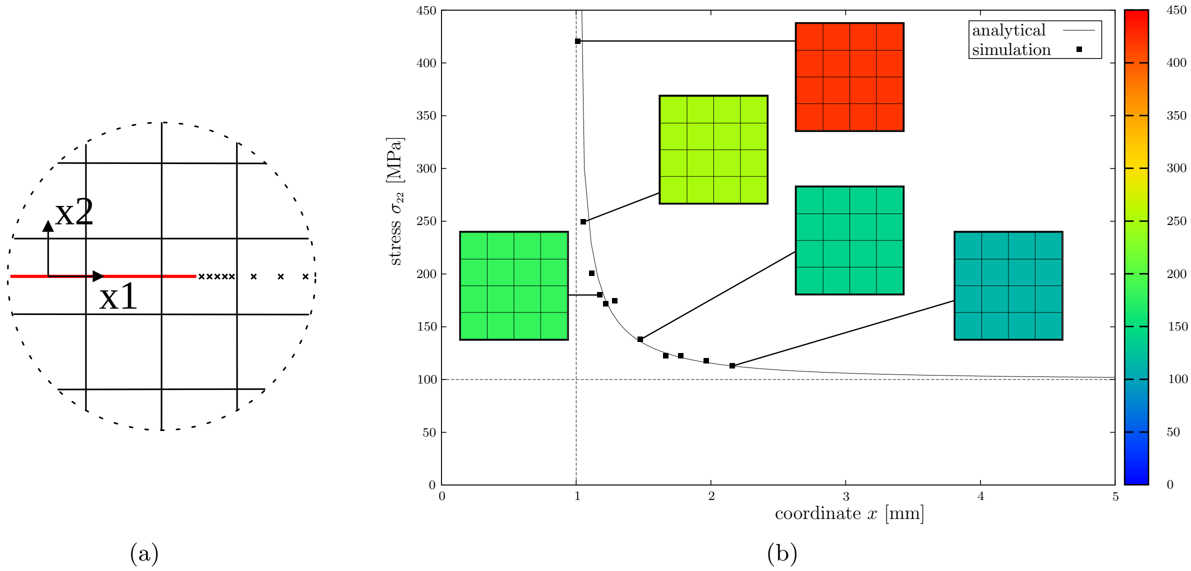

Fig. 4.3-3: (a): FE-mesh in front of crack tip with position of Gaussian points for stress evaluation, (b):Comparison of analytical and numerical solution at macroscale as well as microscopic stress distribution

References

[1] J. Aboudi, *Constitutive behaviour of multiphase metal matrix composites with interfacial damage by the generalized cells model*, in Damage in Composite Materials, G. Z. Voyiadjis, ed., Elsevier Science, 1993.

[2] J. Aboudi, S. Arnold, and B. Bednarcyk, *Micromechanics of Composite Materials: A Generalized Multiscale Analysis Approach*, Elsevier Science, 2012.

[3] J. Aboudi, M.-J. Pindera, and S. M. Arnold, *Linear thermoelastic higher-order theory for periodic multiphase materials*, Journal of Applied Mechanics, 68 (2001), pp. 697–707.

[4] H. Altenbach, J. Altenbach, and R. Rikards, *Einführung in die Mechanik der Laminat- und Sandwichtragwerke*, Deutscher Verlag für Grundstoffindustrie Stuttgart, 1996.

[5] Y. Bansal and M.-J. Pindera, *Testing the predictive capability of the high-fidelity generalized method of cells using an efficient reformulation*, NASA/CR–2004, (2004).

[6] T. Belytschko and T. Black, *Elastic crack growth in finite elements with minimal remeshing*, International Journal for Numerical Methods in Engineering, 45 (1999), pp. 601–620.

[7] T. Belytschko, W. Liu, B. Moran, and K. Elkhodary, *Nonlinear Finite Elements for Continua and Structures*, vol. 2 Auflage, Wiley, 2014.

[8] J. C. Brewer and P. A. Lagace, *Quadratic Stress Criterion for Initiation of Delamination*, Journal of Composite Materials, 22 (1988), pp. 1141–1155.

[9] F. Burbulla, *Kontinuumsmechanische und bruchmechanische Modelle für Werkstoffverbunde:*, Berichte des Instituts für Mechanik, Kassel University Press, 2015.

[10] P. P. Camanho and C. G. Dávila, *Mixed-mode decohesion finite elements for the simulation of delamination in composite materials*, tech. rep., National Aeronautics and Space Administration NASA/TM-2002-211737, 2002.

[11] J. L. Chaboche, R. Girad, and A. Schaff, *Numerical analysis of composite systems by using interphase/interface models*, Computational Mechanics, 20 (1997), pp. 3–11.

[12] J. Dolbow, N. Moës, and T. Belytschko, *Discontinuous enrichment in finite elements with a partition of unity method*, Finite Elements in Analysis and Design, 36 (2000), pp. 235–260.

[13] T. P. Fries and T. Belytschko, *The extended/generalized finite element method: An overview of the method and its applications*, International Journal for Numerical Methods in Engineering, 84 (2010), pp. 253–304.

[14] R. Haj-Ali and J. Aboudi, *A new and general formulation of the parametric hfgmc micromechanical method for two and three-dimensional multi-phase composites*, International Journal of Solids and Structures, 50 (2013), pp. 907–919.

[15] A. Hillerborg, M. Modéer, and P.-E. Petersson, *Analysis of crack formation and crack growth in concrete by means of fracture mechanics and finite elements*, Cement and concrete research, 6 (1976), pp. 773–782.

[16] A. Kaddour, M. Hinton, P. Smith, and S. Li, *The background to the third world-wide failure exercise*, Journal of Composite Materials, 47 (2013), pp. 2471–2426.

[17] A. R. Khoei, *Extended Finite Element Method: Theory and Applications*, Wiley, 2015.

[18] M. Kuna, *Numerische Beanspruchungsanalyse von Rissen, Finite Elemente in der Bruchmechanik*, vol. 2. Auflage, Vieweg + Teubner Verlag, 2010.

[19] B. Kurnatowski, *Zweiskalensimulation von mikroheterogenen Strukturen aus spröden Faserverbundwerkstoffen*, PhD thesis, Kassel University, 2009. in German.

[20] P. Laborde, J. Pommier, Y. Renard, and M. Salaün, *High-order extended finite element method for cracked domains*, International Journal for Numerical Methods in Engineering, 64 (2005), pp. 354–381.

[21] C. J. Lissenden, *An Approximate Representation of Fibre-Matrix Debonding in Nonperiodic Metal Matrix Composites*, In G. Z. Voyiadjis and D. H. Allen, editors, Damage and Interfacial Debonding in Composites, Elsevier Science, 1996, pp. 189–212.

[22] A. Matzenmiller and B. Kurnatowski, *A Comparison of Micromechanical Models for the Homogenization of Microheterogeneous Elastic Composites*, Advances in Mathematical Modeling and Experimental Methods for Materials and Structures. The Jacob Aboudi Volume, (2009), pp. 57–71.

[23] N. Moës, J. Dolbow, and T. Belytschko, *A finite element method for crack growth without remeshing*, International Journal for Numerical Methods in Engineering, 46 (1999), pp. 131–150.

[24] M. Paley and J. Aboudi, *Micromechanical analysis of composites by the generalized cells method*, Mech. Mater., 14 (1992), pp. 127–139.

[25] M.-J. Pindera and B. Bednarcyk, *An efficient implementation of the generalized method of cells for unidirectional, multi-phased composites with complex microstructures*, Composites Part B: Engineering, 30 (1999), pp. 87–105.

[26] R. L. Taylor, *FEAP – A Finite Element Analysis Program*, Department of Civil and Environmental Engineering, University of California at Berkeley, Berkeley, USA, 8.2 ed., March 2008.

[27] J. D. Whitcomb, *Parametric analytical study of instability-related delamination growth*, Comp. Science Tech., 25 (1986), pp. 19–48.

A Components of Subcell-Stiffness Matrix

Solid subcell-stiffness:

$$K_{1,1}^{(\beta\gamma)} = K_{2,2}^{(\beta\gamma)} = \frac{C_{66}^{(\beta\gamma)}}{h_\beta}\left(4 - 3\frac{C_{66}^{(\beta\gamma)}}{\bar{C}_{11}^{(\beta\gamma)}}\right) \tag{A.0-1}$$

$$K_{1,2}^{(\beta\gamma)} = K_{2,1}^{(\beta\gamma)} = \frac{C_{66}^{(\beta\gamma)}}{h_\beta}\left(2 - 3\frac{C_{66}^{(\beta\gamma)}}{\bar{C}_{11}^{(\beta\gamma)}}\right) \tag{A.0-2}$$

$$K_{1,7}^{(\beta\gamma)} = K_{1,8}^{(\beta\gamma)} = K_{2,7}^{(\beta\gamma)} = K_{2,8}^{(\beta\gamma)} = -\frac{3h_\beta C_{55}^{(\beta\gamma)} C_{66}^{(\beta\gamma)}}{l_\gamma^2 \bar{C}_{11}^{(\beta\gamma)}} \tag{A.0-3}$$

$$K_{3,3}^{(\beta\gamma)} = K_{4,4}^{(\beta\gamma)} = \frac{C_{22}^{(\beta\gamma)}}{h_\beta}\left(4 - 3\frac{C_{22}^{(\beta\gamma)}}{\bar{C}_{22}^{(\beta\gamma)}}\right) \tag{A.0-4}$$

$$K_{3,4}^{(\beta\gamma)} = K_{4,3}^{(\beta\gamma)} = \frac{C_{22}^{(\beta\gamma)}}{h_\beta}\left(2 - 3\frac{C_{22}^{(\beta\gamma)}}{\bar{C}_{22}^{(\beta\gamma)}}\right) \tag{A.0-5}$$

$$K_{3,9}^{(\beta\gamma)} = K_{3,10}^{(\beta\gamma)} = K_{4,9}^{(\beta\gamma)} = K_{4,10}^{(\beta\gamma)} = -3\frac{C_{22}^{(\beta\gamma)} C_{44}^{(\beta\gamma)} h_\beta}{\bar{C}_{22}^{(\beta\gamma)} l_\gamma^2} \tag{A.0-6}$$

$$K_{3,11}^{(\beta\gamma)} = -K_{3,12}^{(\beta\gamma)} = -K_{4,11}^{(\beta\gamma)} = K_{4,12}^{(\beta\gamma)} = \frac{C_{23}^{(\beta\gamma)}}{l_\gamma} \tag{A.0-7}$$

$$K_{5,5}^{(\beta\gamma)} = K_{6,6}^{(\beta\gamma)} = \frac{C_{44}^{(\beta\gamma)}}{h_\beta}\left(4 - 3\frac{l_\gamma^2 C_{44}^{(\beta\gamma)}}{h_\beta^2 \bar{C}_{33}^{(\beta\gamma)}}\right) \tag{A.0-8}$$

$$K_{5,6}^{(\beta\gamma)} = K_{6,5}^{(\beta\gamma)} = \frac{C_{44}^{(\beta\gamma)}}{h_\beta}\left(2 - 3\frac{l_\gamma^2 C_{44}^{(\beta\gamma)}}{h_\beta^2 \bar{C}_{33}^{(\beta\gamma)}}\right) \tag{A.0-9}$$

$$K_{5,9}^{(\beta\gamma)} = -K_{5,10}^{(\beta\gamma)} = -K_{6,9}^{(\beta\gamma)} = K_{6,10}^{(\beta\gamma)} = \frac{C_{44}^{(\beta\gamma)}}{l_\gamma} \tag{A.0-10}$$

$$K_{5,11}^{(\beta\gamma)} = K_{5,12}^{(\beta\gamma)} = K_{6,11}^{(\beta\gamma)} = K_{6,12}^{(\beta\gamma)} = -3\frac{C_{33}^{(\beta\gamma)} C_{44}^{(\beta\gamma)}}{h_\beta \bar{C}_{33}^{(\beta\gamma)}} \tag{A.0-11}$$

$$K_{7,1}^{(\beta\gamma)} = K_{7,2}^{(\beta\gamma)} = K_{8,1}^{(\beta\gamma)} = K_{8,2}^{(\beta\gamma)} = -\frac{3C_{55}^{(\beta\gamma)} C_{66}^{(\beta\gamma)}}{l_\gamma \bar{C}_{11}^{(\beta\gamma)}} \tag{A.0-12}$$

$$K_{7,3}^{(\beta\gamma)} = K_{7,4}^{(\beta\gamma)} = 0 \tag{A.0-13}$$

$$K_{7,7}^{(\beta\gamma)} = K_{8,8}^{(\beta\gamma)} = \frac{C_{55}^{(\beta\gamma)}}{l_\gamma}\left(4 - 3\frac{h_\beta^2 C_{55}^{(\beta\gamma)}}{l_\gamma^2 \bar{C}_{11}^{(\beta\gamma)}}\right) \tag{A.0-14}$$

$$K_{7,8}^{(\beta\gamma)} = K_{8,7}^{(\beta\gamma)} = \frac{C_{55}^{(\beta\gamma)}}{l_\gamma}\left(2 - 3\frac{h_\beta^2 C_{55}^{(\beta\gamma)}}{l_\gamma^2 \bar{C}_{11}^{(\beta\gamma)}}\right) \tag{A.0-15}$$

$$K_{9,3}^{(\beta\gamma)} = K_{9,4}^{(\beta\gamma)} = K_{10,3}^{(\beta\gamma)} = K_{10,4}^{(\beta\gamma)} = -3\frac{C_{22}^{(\beta\gamma)} C_{44}^{(\beta\gamma)}}{l_\gamma \bar{C}_{22}^{(\beta\gamma)}} \tag{A.0-16}$$

$$K_{9,5}^{(\beta\gamma)} = -K_{9,6}^{(\beta\gamma)} = -K_{10,5}^{(\beta\gamma)} = K_{10,6}^{(\beta\gamma)} = \frac{C_{44}^{(\beta\gamma)}}{h_\beta} \tag{A.0-17}$$

$$K_{9,9}^{(\beta\gamma)} = K_{10,10}^{(\beta\gamma)} = \frac{C_{44}^{(\beta\gamma)}}{l_\gamma}\left(4 - 3\frac{h_\beta^2 C_{44}^{(\beta\gamma)}}{l_\gamma^2 \bar{C}_{22}^{(\beta\gamma)}}\right) \tag{A.0-18}$$

$$K_{9,10}^{(\beta\gamma)} = K_{10,9}^{(\beta\gamma)} = \frac{C_{44}^{(\beta\gamma)}}{l_\gamma}\left(2 - 3\frac{h_\beta^2 C_{44}^{(\beta\gamma)}}{l_\gamma^2 \bar{C}_{22}^{(\beta\gamma)}}\right) \tag{A.0-19}$$

$$K_{11,3}^{(\beta\gamma)} = -K_{11,4}^{(\beta\gamma)} = -K_{12,3}^{(\beta\gamma)} = K_{12,4}^{(\beta\gamma)} = \frac{C_{23}^{(\beta\gamma)}}{h_\beta} \tag{A.0-20}$$

$$K_{11,5}^{(\beta\gamma)} = K_{11,6}^{(\beta\gamma)} = K_{12,5}^{(\beta\gamma)} = K_{12,6}^{(\beta\gamma)} = -3\frac{l_\gamma C_{33}^{(\beta\gamma)} C_{44}^{(\beta\gamma)}}{h_\beta^2 \bar{C}_{33}^{(\beta\gamma)}} \tag{A.0-21}$$

$$K_{11,11}^{(\beta\gamma)} = K_{12,12}^{(\beta\gamma)} = \frac{C_{33}^{(\beta\gamma)}}{l_\gamma}\left(4 - 3\frac{C_{33}^{(\beta\gamma)}}{\bar{C}_{33}^{(\beta\gamma)}}\right) \tag{A.0-22}$$

$$K_{11,12}^{(\beta\gamma)} = K_{12,11}^{(\beta\gamma)} = \frac{C_{33}^{(\beta\gamma)}}{l_\gamma}\left(2 - 3\frac{C_{33}^{(\beta\gamma)}}{\bar{C}_{33}^{(\beta\gamma)}}\right) . \tag{A.0-23}$$

Elastic subcell-stiffness:

$$D_{15}^{(\beta,\gamma)} = -D_{25}^{(\beta,\gamma)} = 2C_{66}^{(\beta,\gamma)} \tag{A.0-24}$$

$$D_{31}^{(\beta,\gamma)} = -D_{41}^{(\beta,\gamma)} = C_{12}^{(\beta,\gamma)} \tag{A.0-25}$$

$$D_{32}^{(\beta,\gamma)} = -D_{42}^{(\beta,\gamma)} = C_{22}^{(\beta,\gamma)} \tag{A.0-26}$$

$$D_{33}^{(\beta,\gamma)} = -D_{43}^{(\beta,\gamma)} = D_{11,2}^{(\beta,\gamma)} = -D_{12,2}^{(\beta,\gamma)} = C_{23}^{(\beta,\gamma)} \tag{A.0-27}$$

$$D_{54}^{(\beta,\gamma)} = -D_{64}^{(\beta,\gamma)} = D_{94}^{(\beta,\gamma)} = -D_{10,4}^{(\beta,\gamma)} = 2C_{44}^{(\beta,\gamma)} \tag{A.0-28}$$

$$D_{76}^{(\beta,\gamma)} = -D_{86}^{(\beta,\gamma)} = 2C_{55}^{(\beta,\gamma)} \tag{A.0-29}$$

$$D_{11,1}^{(\beta,\gamma)} = -D_{12,1}^{(\beta,\gamma)} = C_{13}^{(\beta,\gamma)} \tag{A.0-30}$$

$$D_{11,3}^{(\beta,\gamma)} = -D_{12,3}^{(\beta,\gamma)} = C_{33}^{(\beta,\gamma)} . \tag{A.0-31}$$